The Abdus Salam International Centre for Theoretical Physics

United Nations Educational, Scientific and Cultural Organization
IAEA
International Atomic Energy Agency

1865-6

School on Astrophysical Fluid Dynamics

15 - 26 October 2007

Computational Astrophysics

Silvano Massaglia
Universita' di Torino, Italy

Strada Costiera 11, 34014 Trieste, Italy - Tel. +39 040 2240 111; Fax +39 040 224 163 - sci_info@ictp.it, www.ictp.it

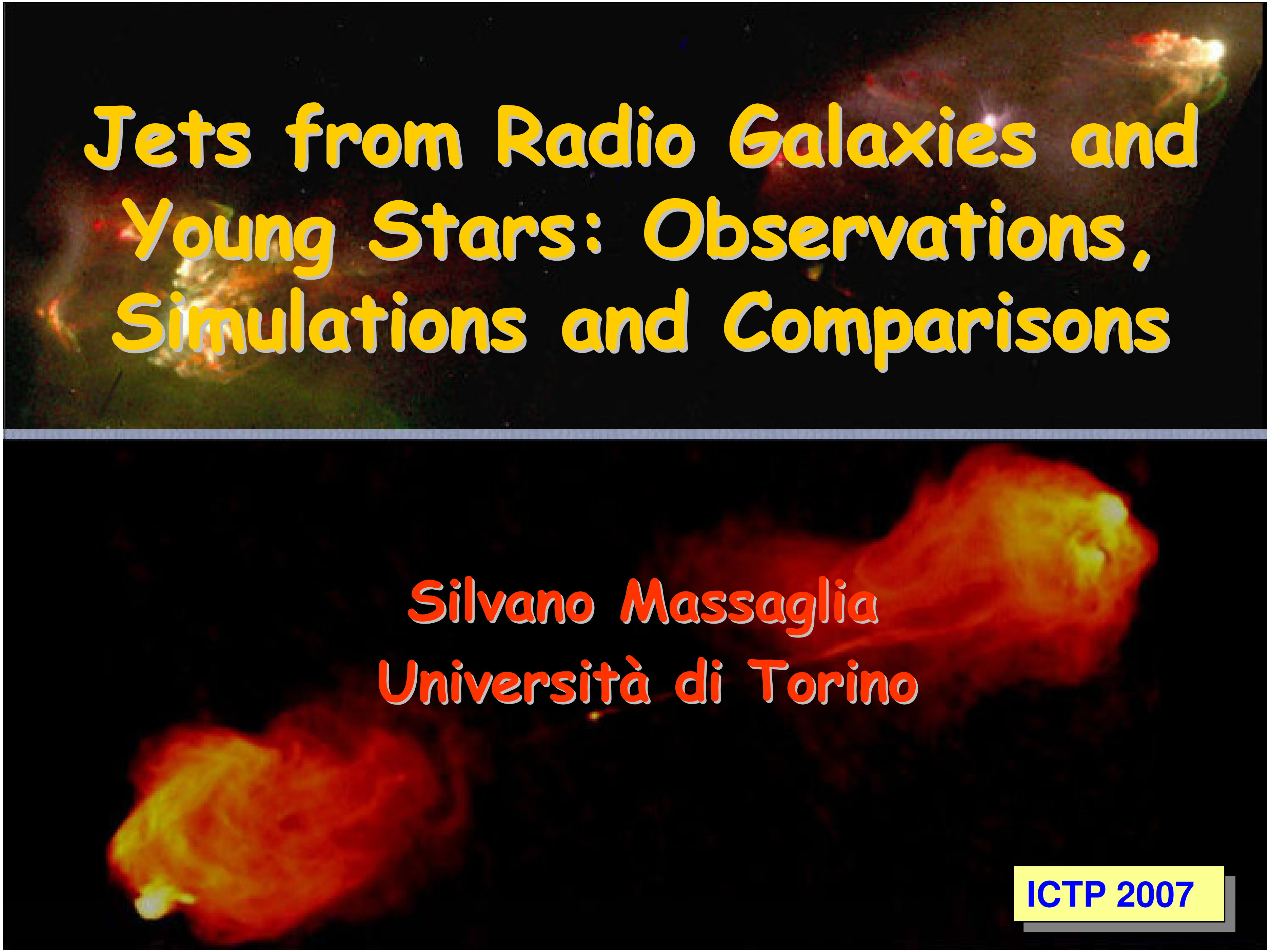
Jets from Radio Galaxies and Young Stars: Observations, Simulations and Comparisons
Silvano Massaglia
Università di Torino
ICTP 2007

Overview

- Radio Galaxies: Main facts
- Constraining the physical parameters in RGs
- Numerical simulations of jets in radio galaxies: comparison with observations
- Stellar jets and their environment: Main facts
- Constraining the physical parameters in YSO jets
- Numerical simulations of YSO jets: comparison with observations
- Jet acceleration mechanisms
- Conclusions

Astrophysical Jets

Collimated outflows in form of jets are ubiquitous in the Universe:

1. Jets from AGNs in Radio Galaxies;
2. binary systems;
3. from Young Stellar Objects;
4. in SS433;
5. from the Crab Pulsar;
6. in the sources of Gamma Ray Bursts

About Radio Galaxies

Synchrotron Radio to X-rays

Radio emission Synchrotron:
$F(\nu) \propto \nu^{-\alpha}$
$\alpha \sim 0.5$

Electron power law distribution
$n(E) \propto E^{-p}$
$p=2\alpha+1$

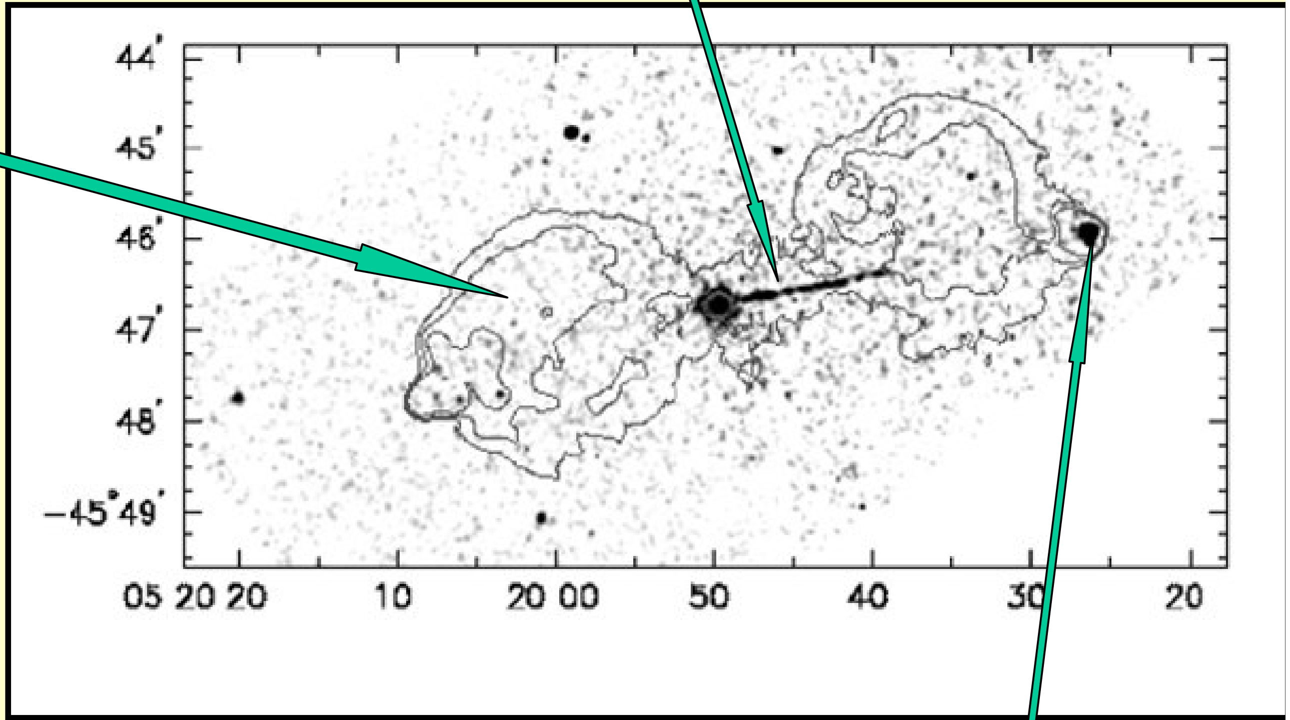

Pictor A (z=0.035)
Nucleus to hot-spot ~ 270 kpc
jet ~ 120 kpc

Radio: synchrotron X-rays: synchrotron+SSC

Radio Galaxies: Main facts

What we know:

- Radio luminosity: 10^{41}-10^{44} ergs s^{-1}
- Size: a few kpc – some Mpc
- Morphologies
- Polarization degree: about 1%-30%

What we guess (but do not know for sure!):

- Life timescale: 10^{7}-10^{8} ys
- Magnetic field: 10 – 10^{3} μG
- Kinetic power: 10^{44}-10^{47} ergs s^{-1}
- Jet Mach number: M>1
- Jet velocity: possibly relativistic
- Jet density: 10^{-5}-10^{-4} cm^{-3}

Radio Galaxies: Main facts

Why these uncertainties in constraining the basic parameters?:

Absence of any line in the radiation spectrum!

Parameters are constrained by indirect means:

- **Magnetic field: by minimum energy condition (equipartition)**
- **Kinetic power: energy requirements**
- **Jet Mach number: indication of shocks**
- **Jet velocity: jet one-sidedness**
- **Jet density: jet numerical modelling**

Observed morphologies:
The Fanaroff-Riley classification

FR I or jet dominated

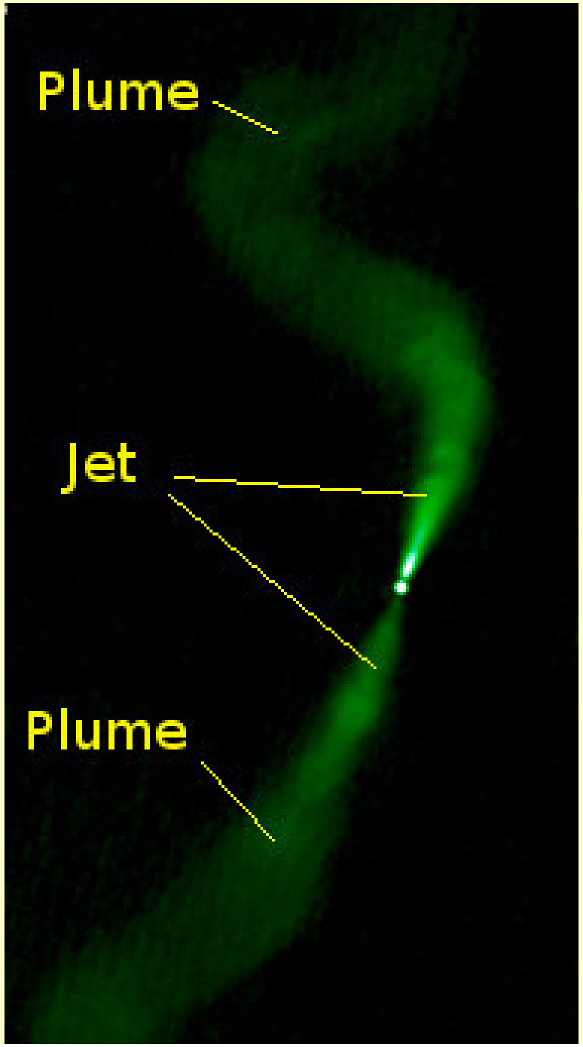

3C 31
VLA

FR II or lobe dominated (classical doubles)

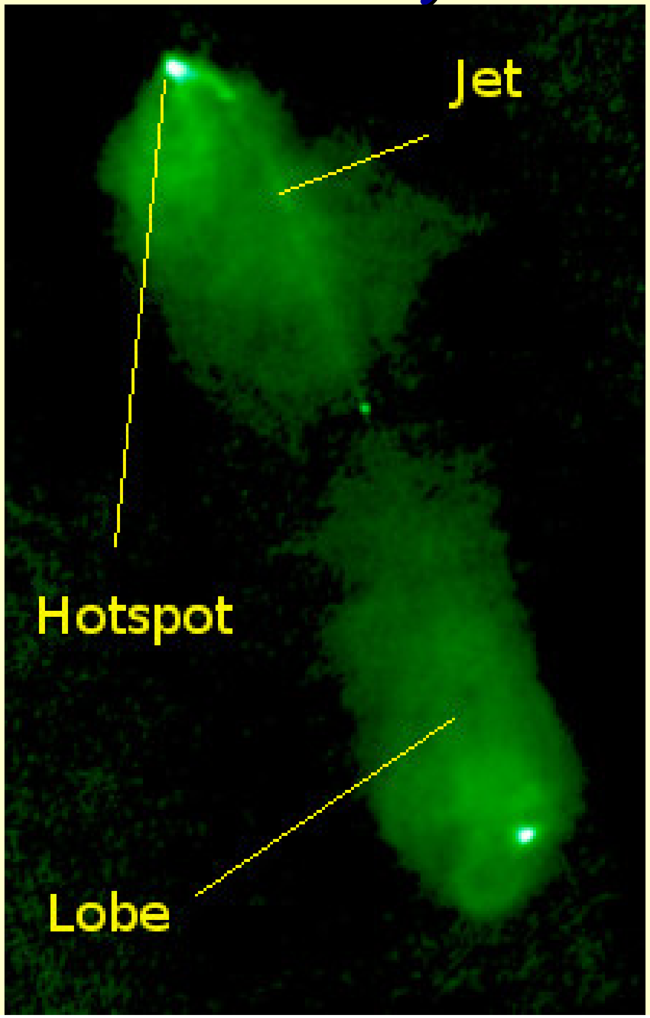

3C 98
VLA

FR II only have Hot-spots!

- FR I: Jet dominated emission, two-sided jets, typically in clusters, weak-lined galaxies
- FR II: Lobe dominated emission, one-sided jets, isolated or in poor groups, strong emission lines galaxies

Radio vs optical luminosities:

$$L_R \propto L_{opt}^{1.7}$$

(Owen & Ledlow 1994)
Environment plays a role?

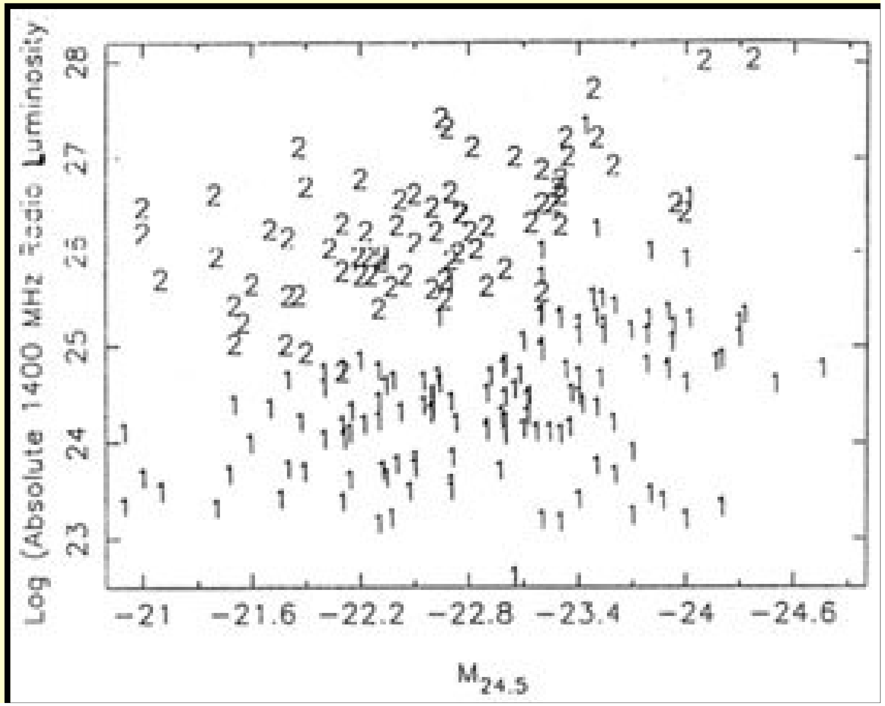

Basic physical parameters

Theoretical modeling and numerical simulations of jets on large scale require a minimum set of parameters:

1. Lorentz factor (Γ)
2. Jet Mach number (M)
3. Jet-ambient density ratio (η)

Velocity: jet one-sidedness

Flux ratio of the approaching (isotropic) jet to the receding one (*Doppler boosting*):

$$\frac{F_a}{F_r} = \left(\frac{1+\beta_j \cos\theta}{1-\beta_j \cos\theta}\right)^{2+\alpha}$$

With $F \propto \nu^{-\alpha}$.

Apparent *vs* intrinsic speed:

$$\beta_{app} = \frac{\beta_j \sin\theta}{1-\beta_j \cos\theta}$$

In principle, one can solve for β_j and θ.

NGC 4261

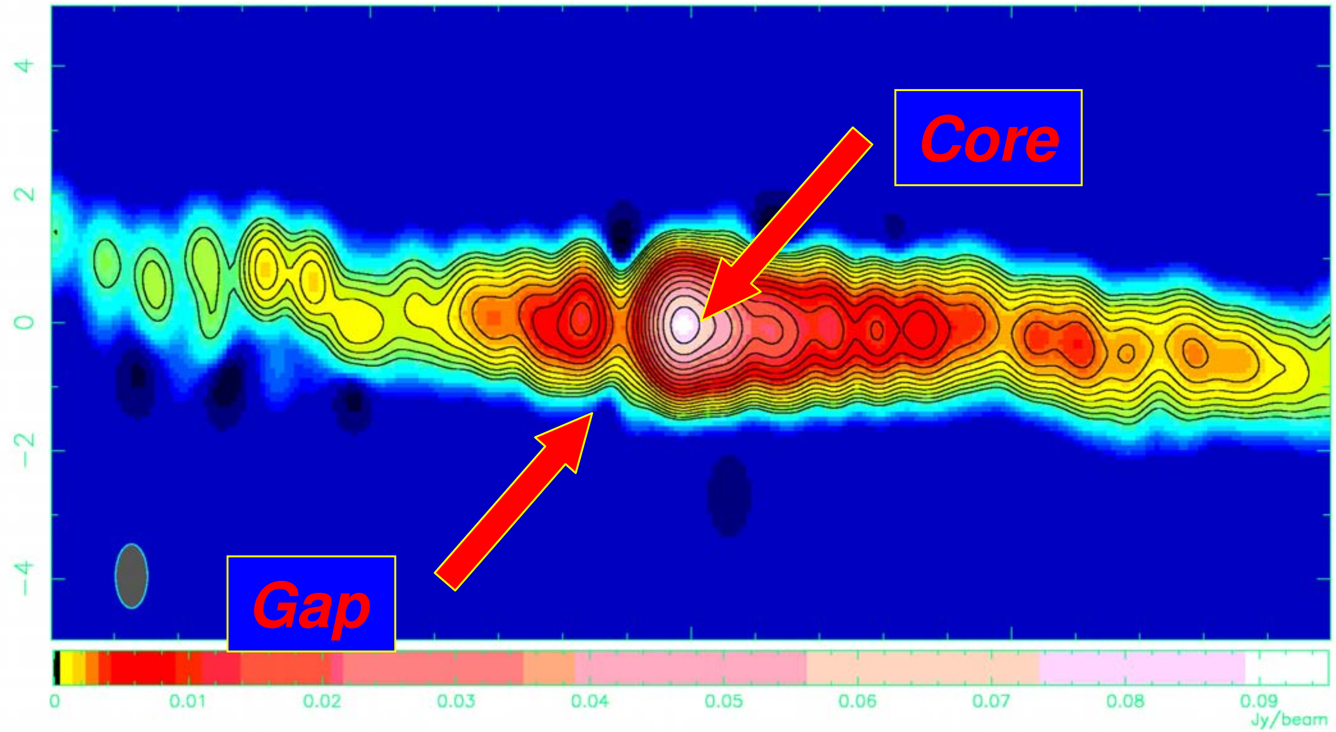

FIG. 2.— Super-resolved false color CLEAN image of NGC 4261 from the 8.4 GHz VLBA observation on 1999 October 21. The displayed region extends to ±10 mas from the presumed core in right ascension, and ±5 mas in declination. The gap in emission is clearly visible 1 mas east of the core. The restoring beam has a FWHM of 1.0 × 0.5 mas. The lowest contour represents a flux density of 0.3 mJy beam^{-1}, and successive contours are each a factor of $\sqrt{2}$ higher.

Jet and counterjet are both visible and proper motions detected: β=0.46±0.02, θ=63±3°

(Piner et al. 2002)

Difficulties…

1. The counterjet is not visible in most cases
2. Proper motions observed in few objects only

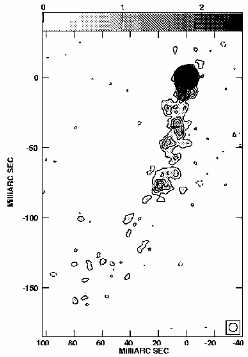

Fig. 9.— VLBA image of 0331+39 with natural weight at 5 GHz. The HPBW is 6 mas. The noise level is 0.08 mJy/beam and levels are: -0.25, 0.25, 0.5, 0.75, 1, 1.5, 3, 5, 10, 20, 30, 50, 70 and 100 mJy/beam.

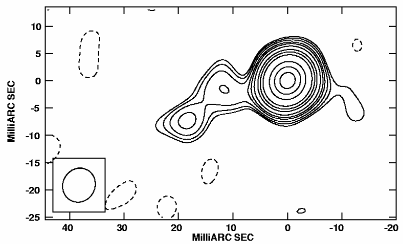

Fig. 11.— VLBA image of 0648+27 at 5 GHz. The HPBW is 6.4 × 5.9 mas (PA -30°). The noise level is 0.2 mJy/beam and levels are: -0.5, 0.5, 0.7, 1, 1.5, 2, 3, 5, 7, 10, 20, 30 and 40 mJy/beam.

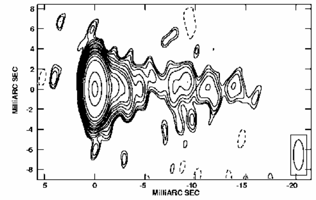

Fig. 15.— Global VLBI image of 1441+52 (3C303) at 5 GHz. The HPBW is 3 × 1 mas in PA 0°. The noise level is 0.05 mJy/beam and levels are: -0.1, 0.1, 0.12, 0.15, 0.2, 0.3, 0.4, 0.6, 0.8, 1, 1.5, 2, 3, 5, 10, 50, and 100 mJy/beam.

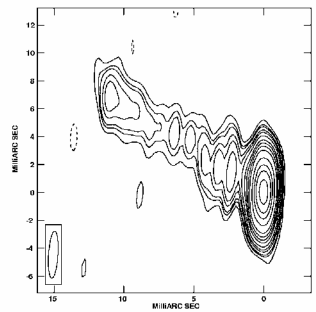

Fig. 16.— Global VLBI image of 1833+32 (3C382) at 5 GHz. The HPBW is 3.4 × 0.7 mas in PA = -4°. The noise level is 0.15 mJy/beam and levels are: -0.5, 0.5, 0.8, 1, 1.5, 2, 3, 5, 7, 10, 15, 30, 50, 70, and 100 mJy/beam.

Jet Mach number: indication of shocks

Pictor A

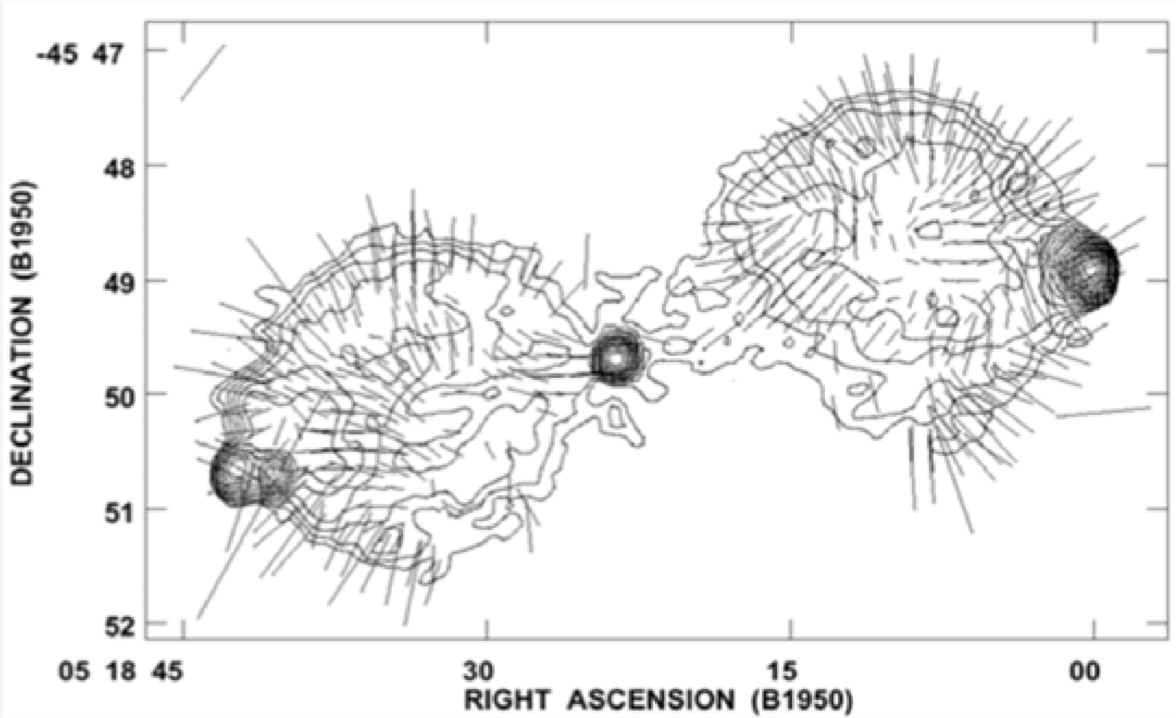

The implied direction of the magnetic field in this image is perpendicular to the straight lines. That is, the magnetic field has a circumferential direction with respect to the plasma in the lobe.

Jet Mach number: indication of shocks

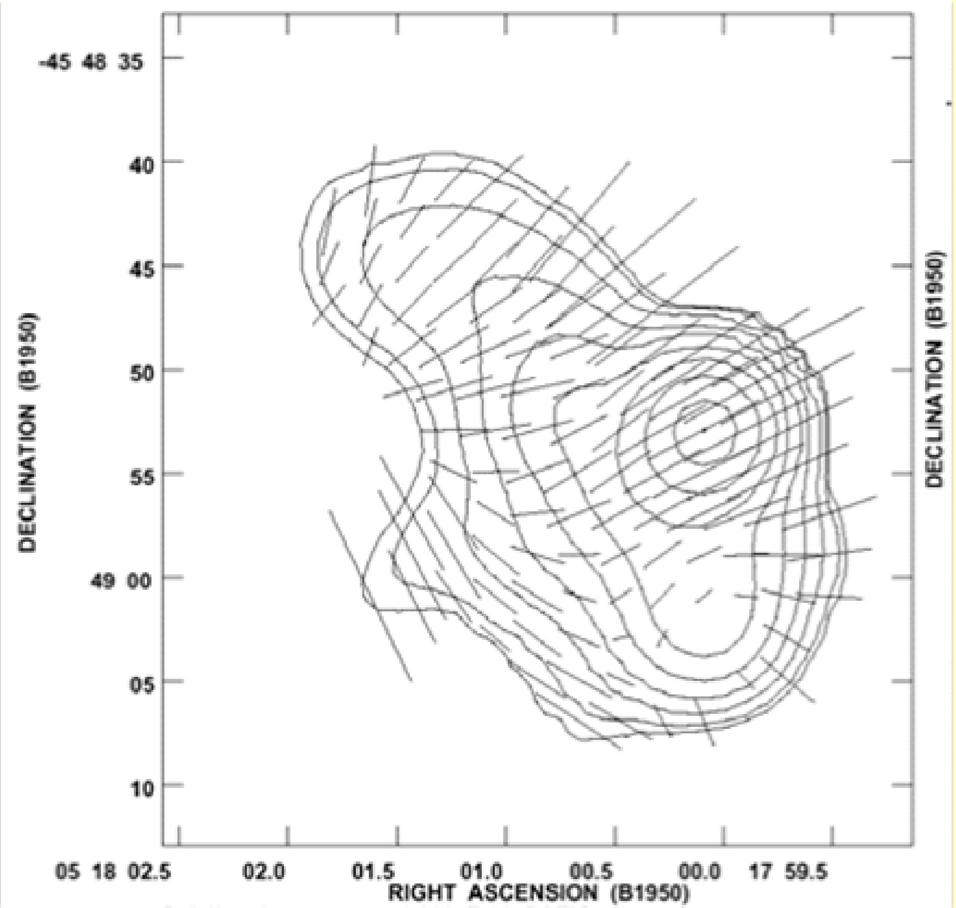

Polarization of the western hot spot of Pictor A, at 3.6 cm wavelength with 400 resolution (left), and at 0.77 by 0.17 resolution (right). The lower resolution map shows the general features of this region, and is contoured at 0.391% and then with a spacing of a factor of 2 between 0.552 and 70.71% of the maximum intensity of 1.55 Jy/beam. The dashed lines again indicate the plane of the electric vector. Their lengths are proportional to the degree of polarization, with 100 equal to 6.67%.

The western hot spot of Pictor A

$B_{eq}=4.6\times10^{-4}$ G

Jet Mach number: indication of shocks

The polarisation of the hot spot in Pictor A reveals magnetic field structure that is consistent with that produced by a shock wave.

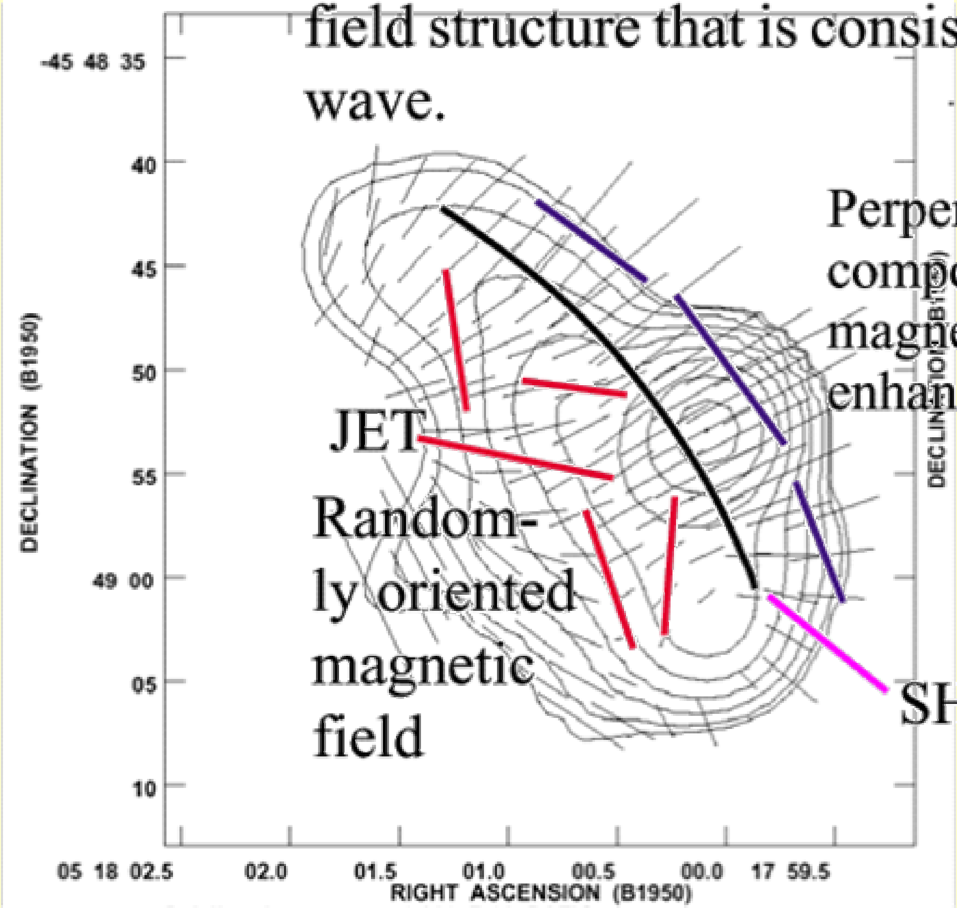

At the terminal shock of the jet, the component of the magnetic field perpendicular to the shock is amplified, whilst leaving the parallel component unchanged. This lines the field up with the shock as shown

Observations of FR II hot-spots

3C445 at the VLT I-band (0.9 μm) (Prieto et al. 2003)

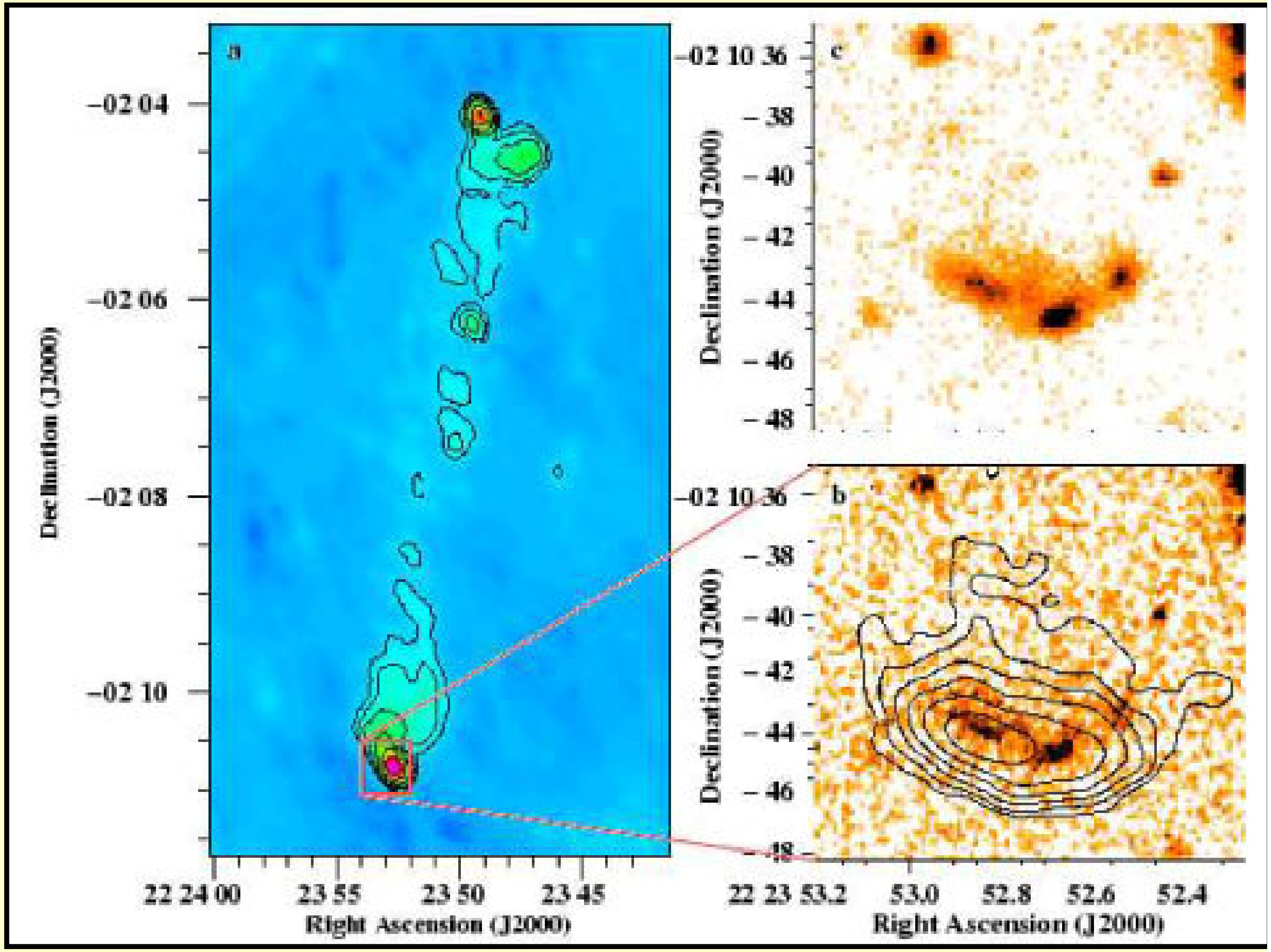

FR II hot-spots

Synchrotron models

K, H, J and I bands and radio flux at 8.4GHz

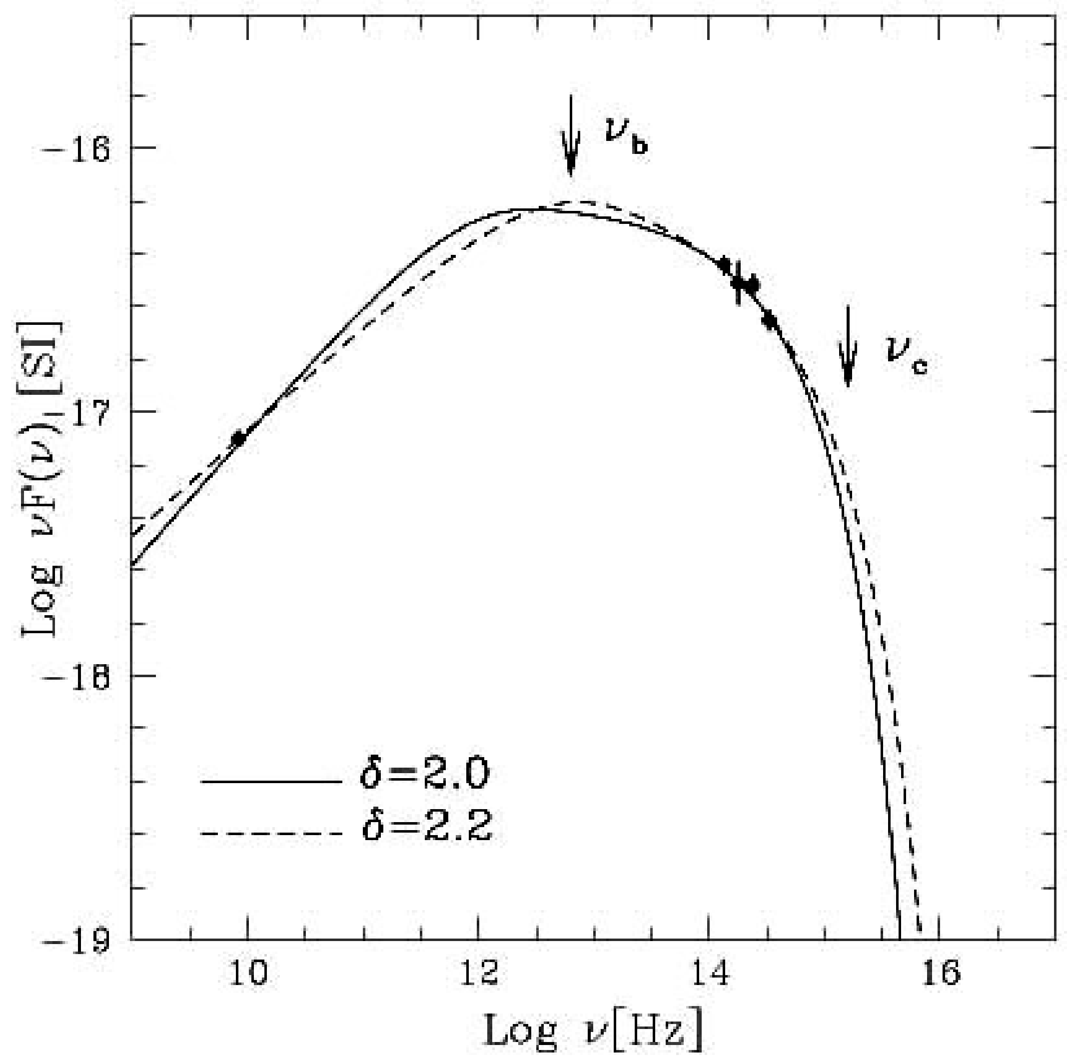

Modelling the jet termination in FR II sources

Bow-shock

Mach disk: possible cosmic ray acceleration site

Contact discontinuity

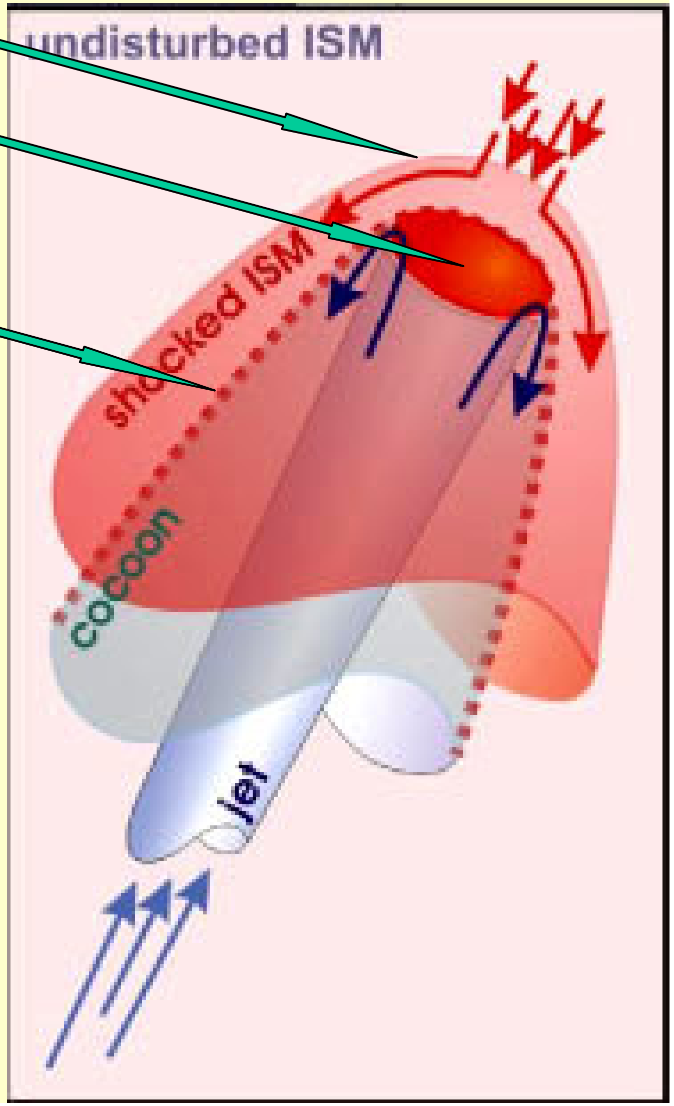

- AGN (FRII) jets are supersonic (M>1)
- Emission non-thermal
- Comparison of model B with B_{eq}

Modelling the jet termination in FR II sources

Terminal shock

jet

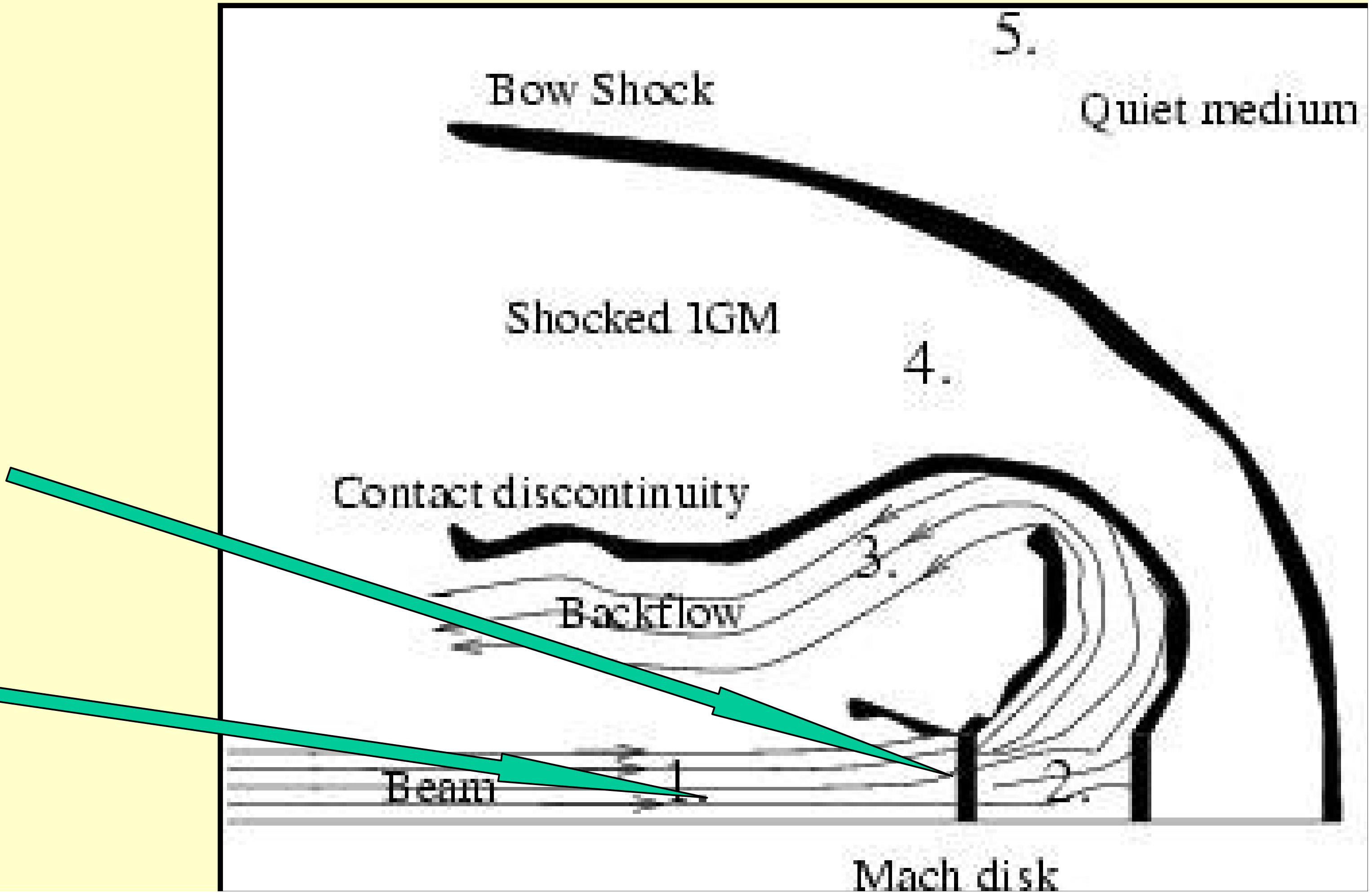

Jet density from FRII morphologies

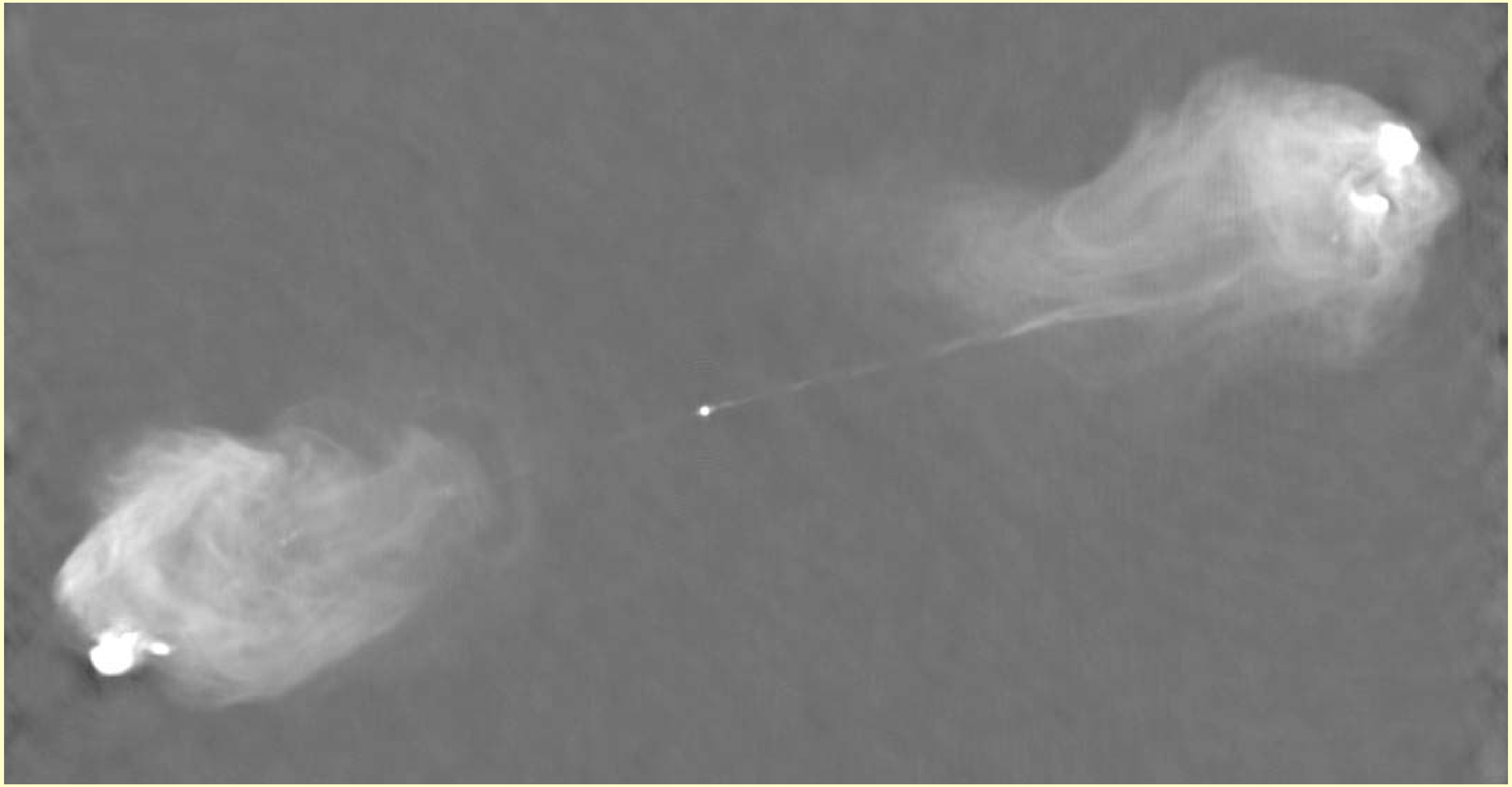

Cygnus A (FR II) - VLA, 6cm

Jet density from FRII morphologies

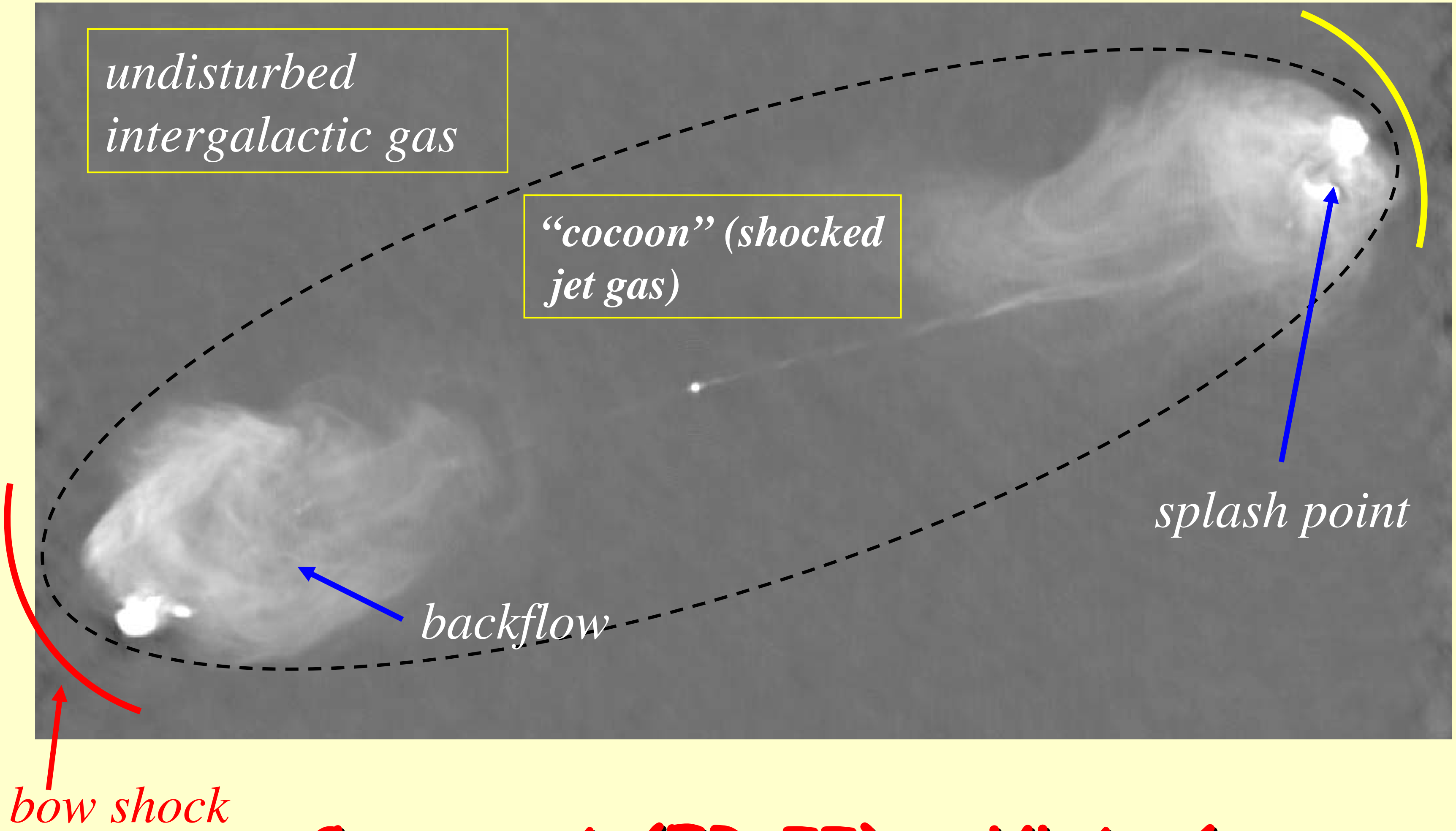

Cygnus A (FR II) - VLA, 6cm

Numerical simulations of FR II

Supersonic and Underdense jet

We use the (M)HD code PLUTO, based on high resolution shock-capturing schemes.
(http://plutocode.to.astro.it)

Numerical simulations of FR II sources

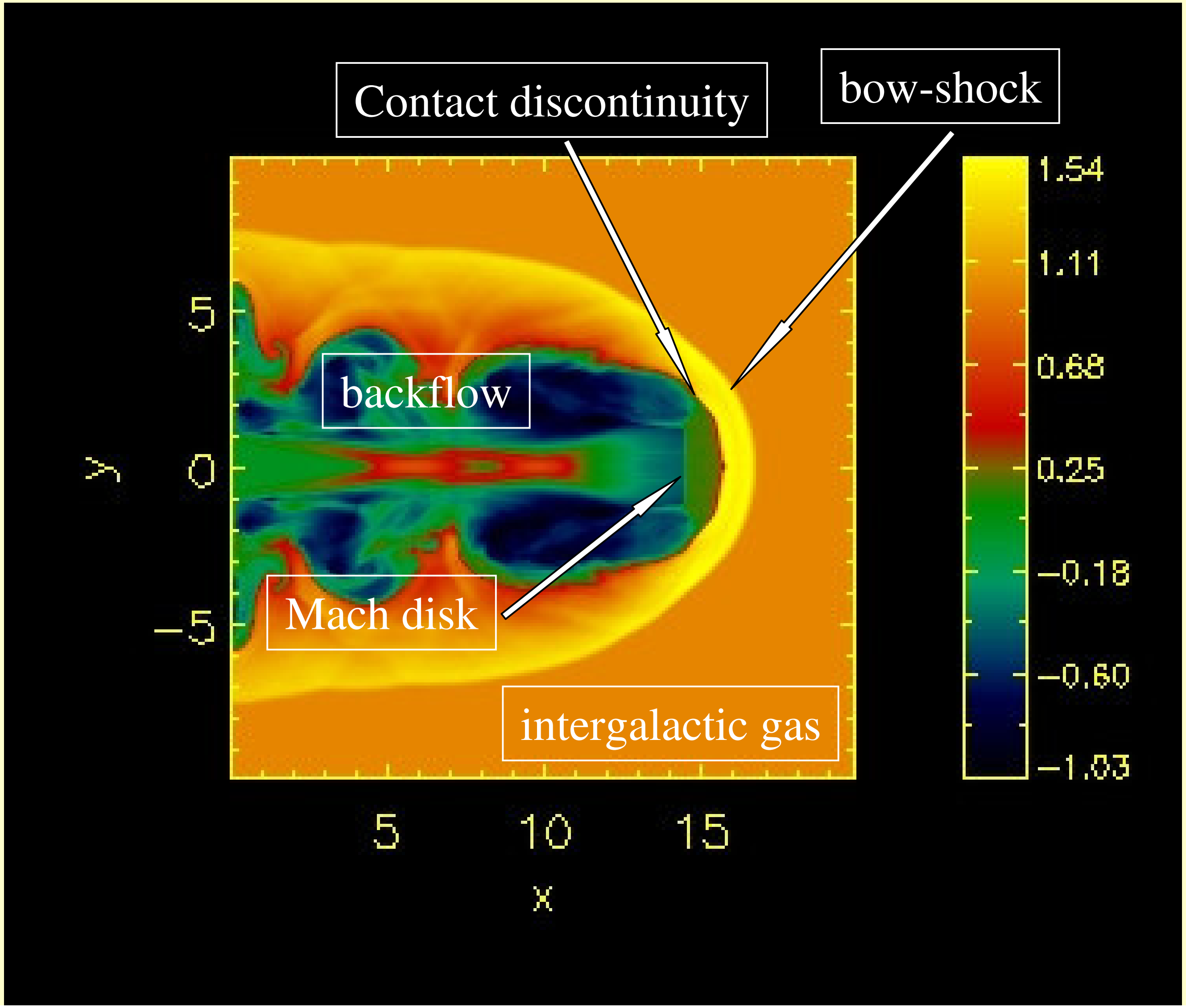

Numerical simulations of FR II

Comparison of observed and simulated morphologies

1. Relativistic (one-sidedness), $\Gamma > 1$
2. Supersonic (presence hot-spots), $M > 1$
3. Underdense (presence of cocoons), $\eta < 1$ (simulations)

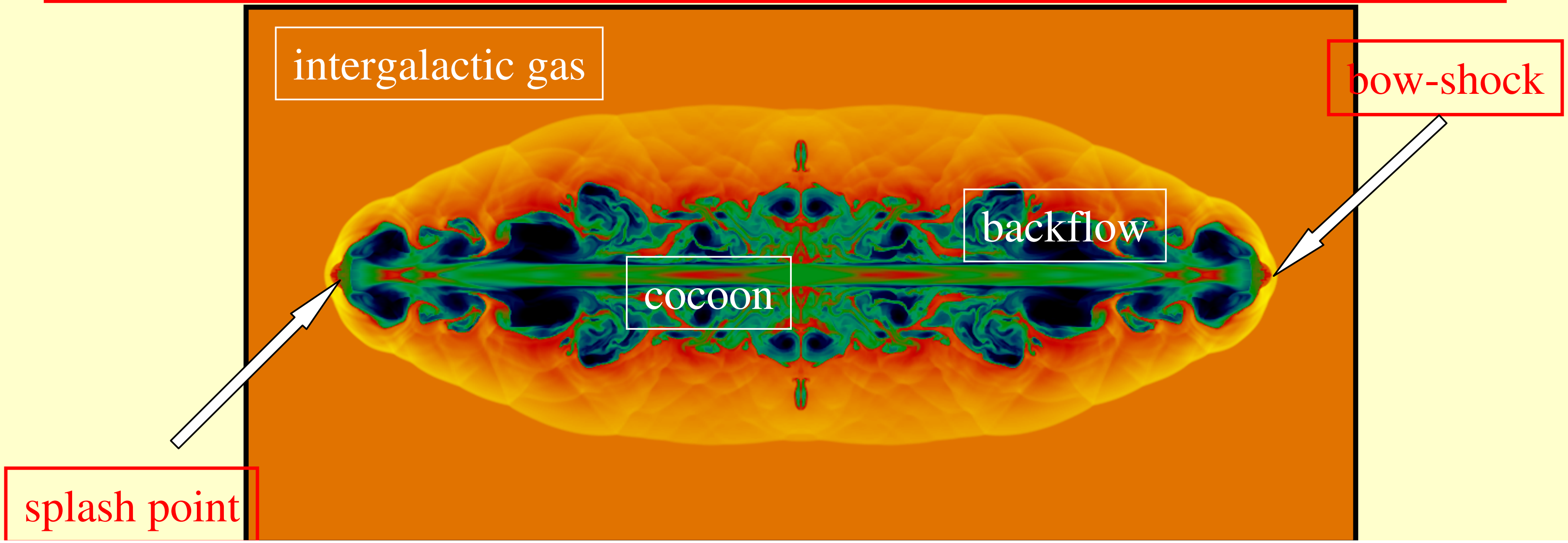

On FR I / FR II Dichotomy

- **Intrinsic explanations:**

1. Differences in jet composition (e^+-e^- for FR I sources, Reynolds et al. 1996a);
2. Difference in the central engine (a fast spinning BH yields FR II jets, Meier 1999)
3. ADAF produce FR I (and BL Lacs), while 'standard' accretion discs FR II (and quasars) (Reynolds et al. 1996b).

- **Extrinsic explanations:**

1. Jets decelerated by instabilities and/or entrainment in weaker jets to produce FR I, stronger jets remain stable to form FR II (Komissarov 1990).
2. Observations of six Hybrid Morphology Radio Sources (HYMORS): FR I on one side of the core and FR II on the other one (Gopal-Krishna & Wiita 2000).

How About FRIs?

FR Is as well are relativistic on the parsec scale

Problem: jet deceleration from the VLBI to VLA scale (see Bowman et al. 1996)

VLBI

VLA

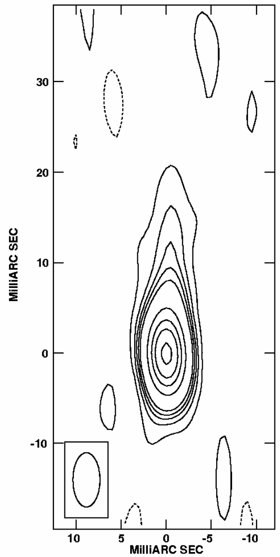

Fig. 13.— Global VLBI image of 1222+13 (3C272.1) at 1.7 GHz. The HPBW is 6 × 3 mas in PA 0°. The noise level is 0.5 mJy/beam and levels are: -1, 1, 3, 5, 7, 10, 30, 50, 70, and 100 mJy/beam.

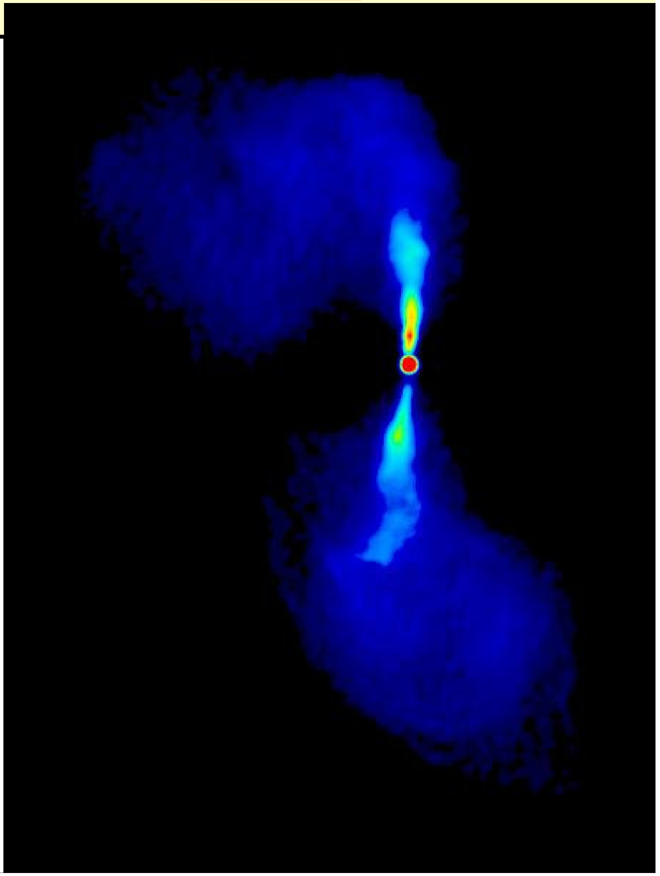

Hymors

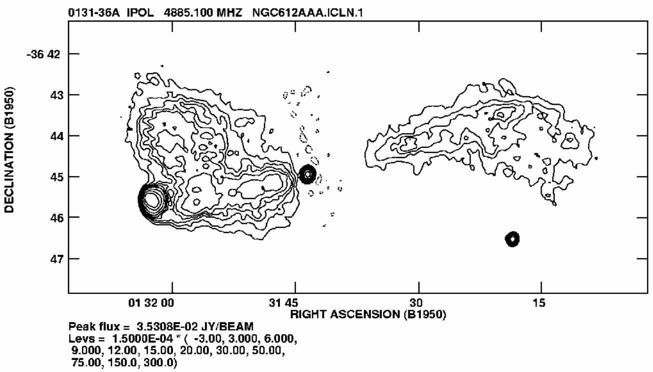

Fig. 1. Maps reproduced from the literature showing the hybrid morphology of some double radio sources: 0131−367, reprinted with permission from Morganti et al. (1993), copyright, Royal Astronomical Society.

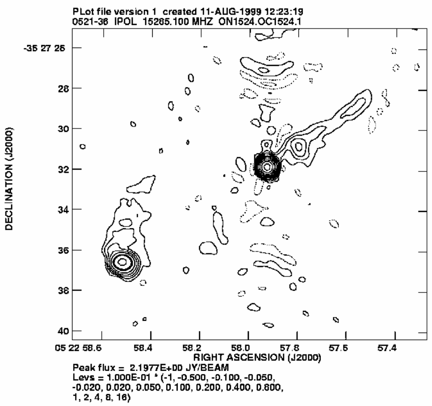

Fig. 2. 0521−364, reprinted with permission from Keel (1996), copyright, American Astronomical Society.

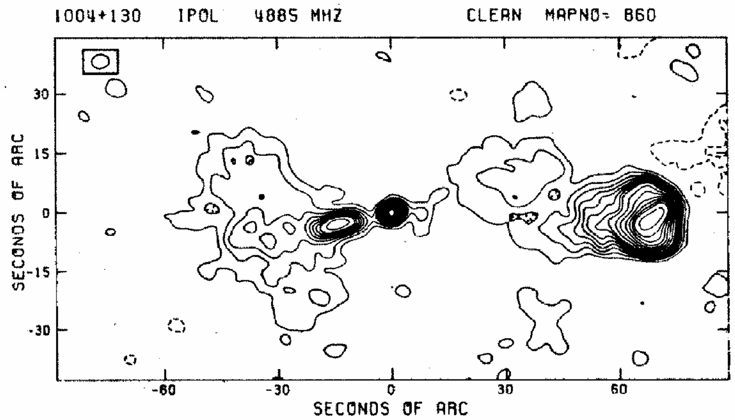

Fig. 3. 1004+130, reprinted with permission from Fomalont (1982), copyright, Kluwer Academic Publishing.

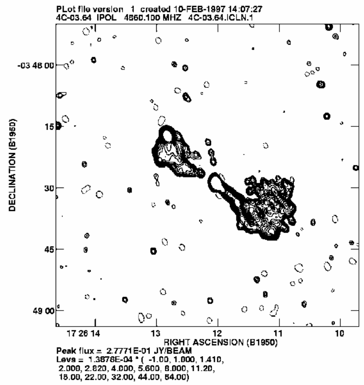

Fig. 4. 1726−038, reprinted with permission from Jackson et al. (1999), copyright, European Southern Observatory.

Jet instability and braking in FRIs

Jet instabilities: linear growth $\tau_{\mathrm{KH}} \sim 2\pi\, M_{\mathrm{J}}\, R_{\mathrm{J}} / c_{\mathrm{s}}$

↓

Nonlinear growth: $\tau_{\mathrm{KH}} \leq 10\, R_{\mathrm{J}} / c_{\mathrm{s}}$

↓

Mixing and mass entrainment

↓

Jet braking

Jet instability and braking in FRIs: Numerical simulations

$$\frac{\rho_{jet}}{\rho_{amb}} = 10^{-4}$$

$$M = \frac{v_j}{c_s} = 3$$

$$\Gamma = 10$$

Jet instability and braking in FRIs: Numerical simulations

Longitudinal behavior of maximum and averaged Lorentz factor

$$\frac{\rho_{jet}}{\rho_{amb}} = 10^{-4}$$

$$M = \frac{v_j}{c_s} = 3$$

$$\Gamma = 10$$

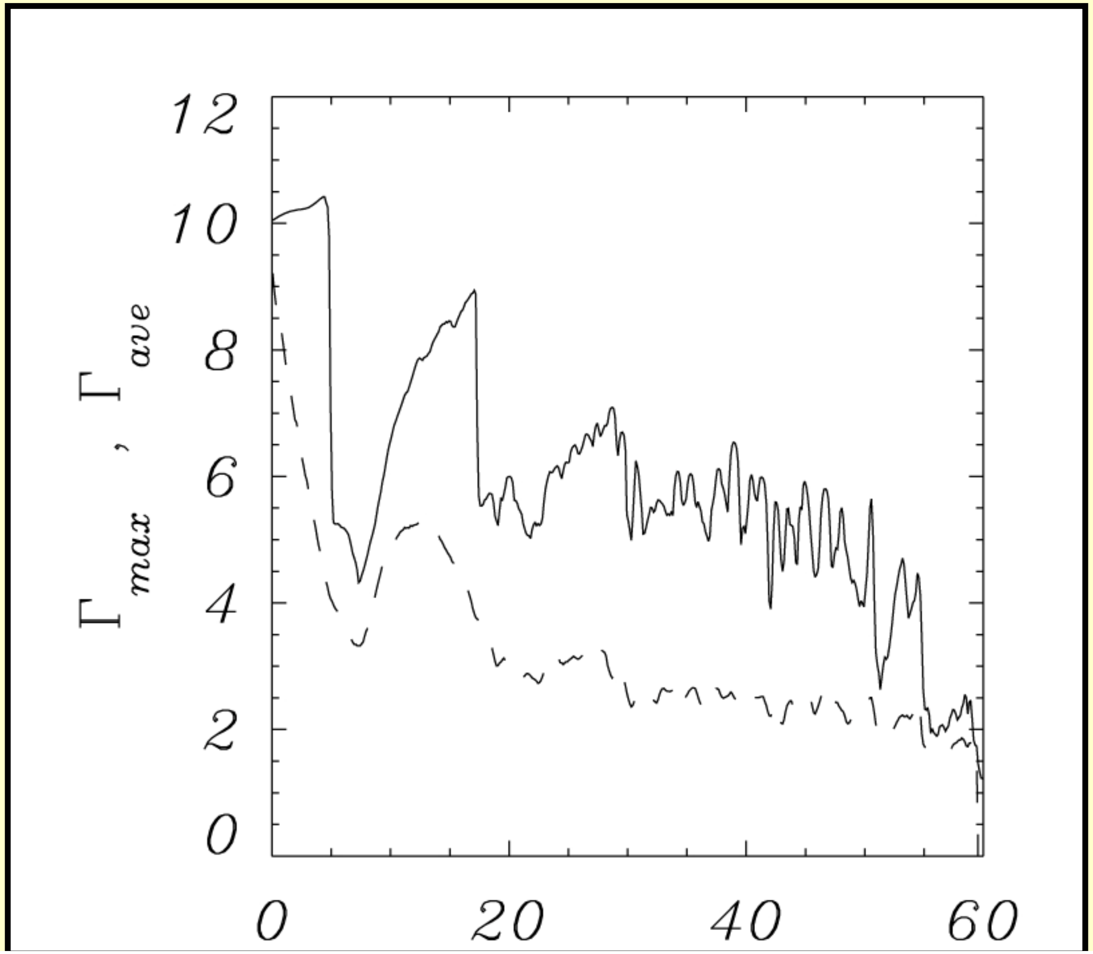

Summary of AGN Jets

- Basic physical parameters are still unconstrained.
- Limits from observations of morphologies.
- Numerical simulations important for the comparison with observations.

The environment of jets from Young Stellar Objects (YSOs)

Located in the *Giant Molecular Clouds*

Giant Molecular Clouds (GMCs) sites star formation.

GMC physical parameters:

1. T~10K
2. density ~1000 times mean ISM.
3. L ~1-100 pc
4. M ~$10^5 - 10^7 M_\odot$
5. *τ* ~10^7 ys

About 1000 GMCs are present in the Milky Way.

Initial phases: from cloud to protostar

T Tauri stars: M~ 0.3-3 $M_\odot$

Phases associated to the presence of jets {

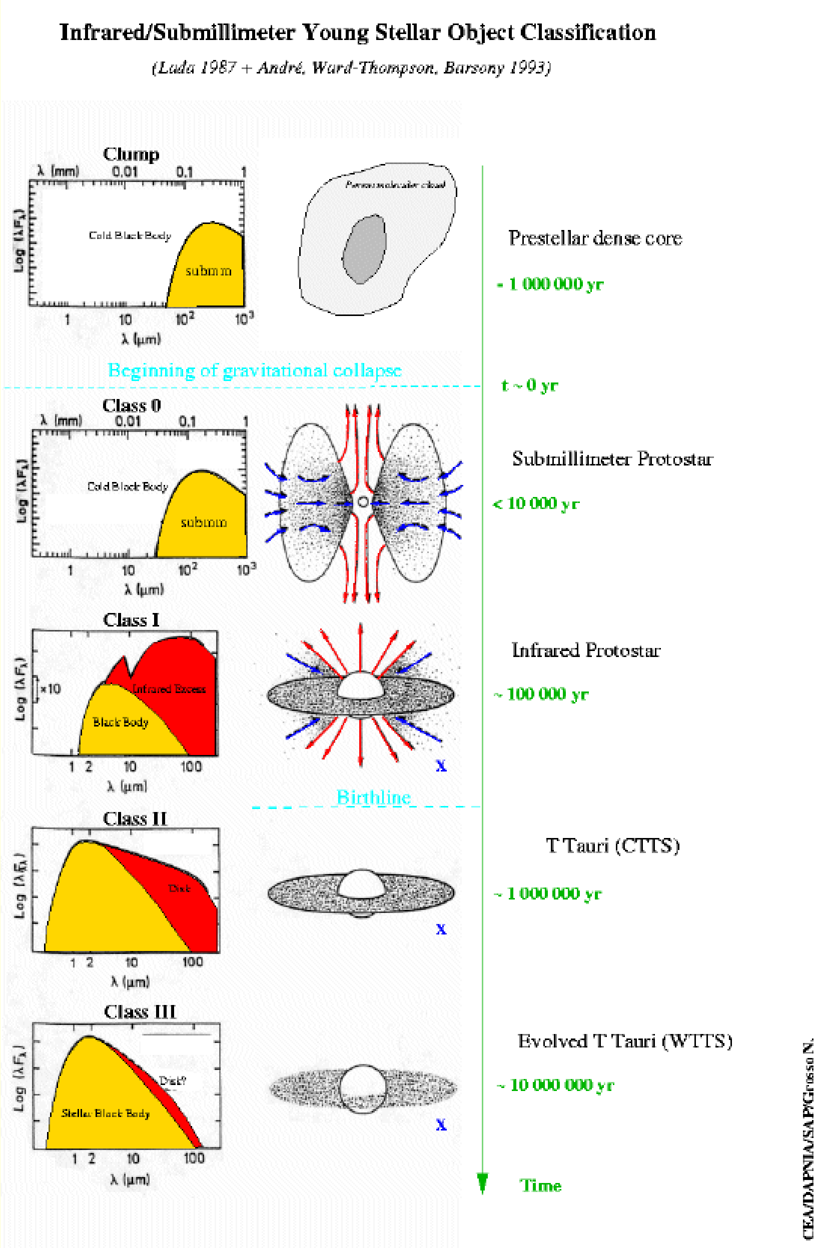

The stellar jets

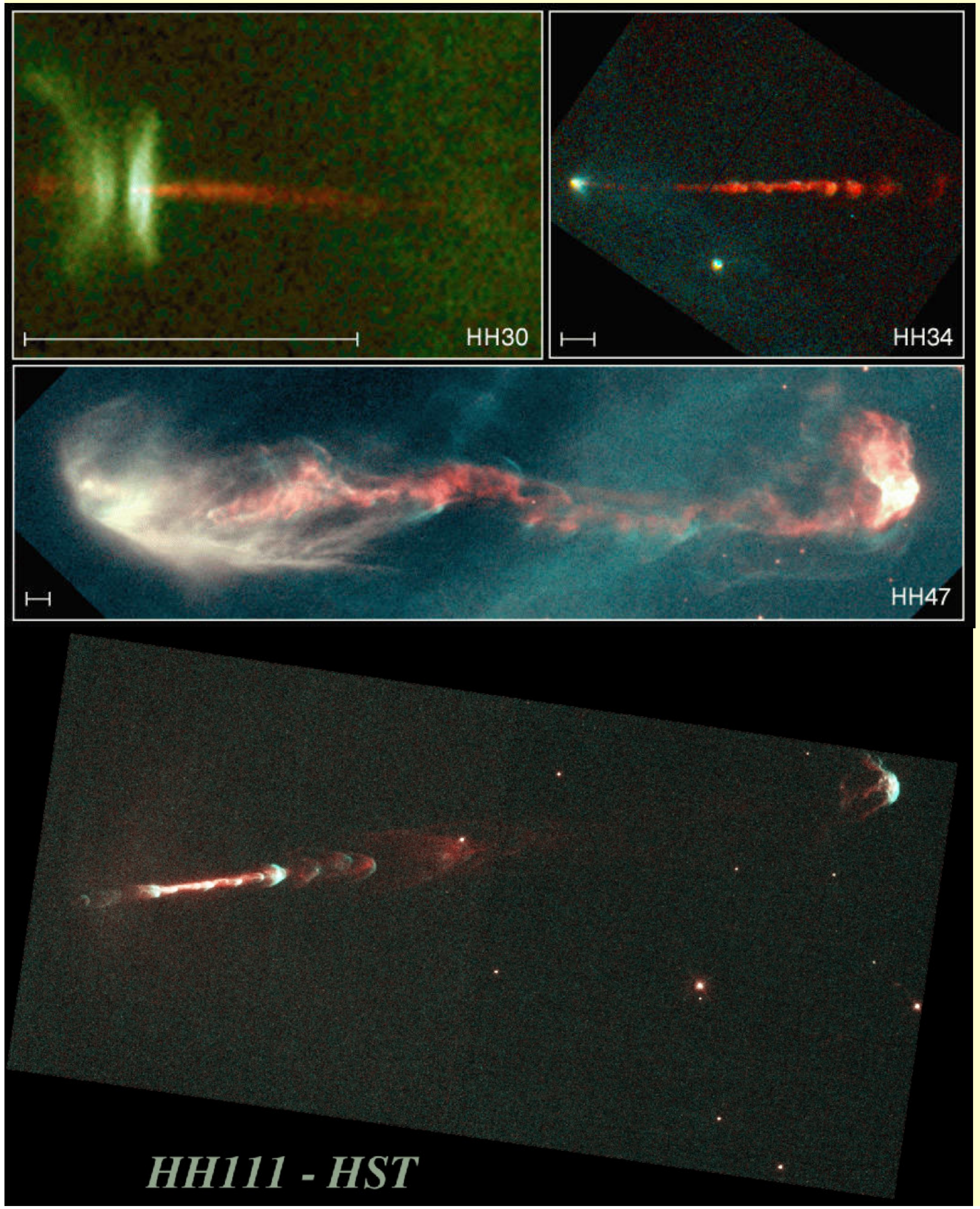

The show to observations:

- ✓ Forbidden emission lines in the optical
- ✓ IR emission
- ✓ Series of knots along the jet at different distances from the source
- ✓ Terminal hot-spots

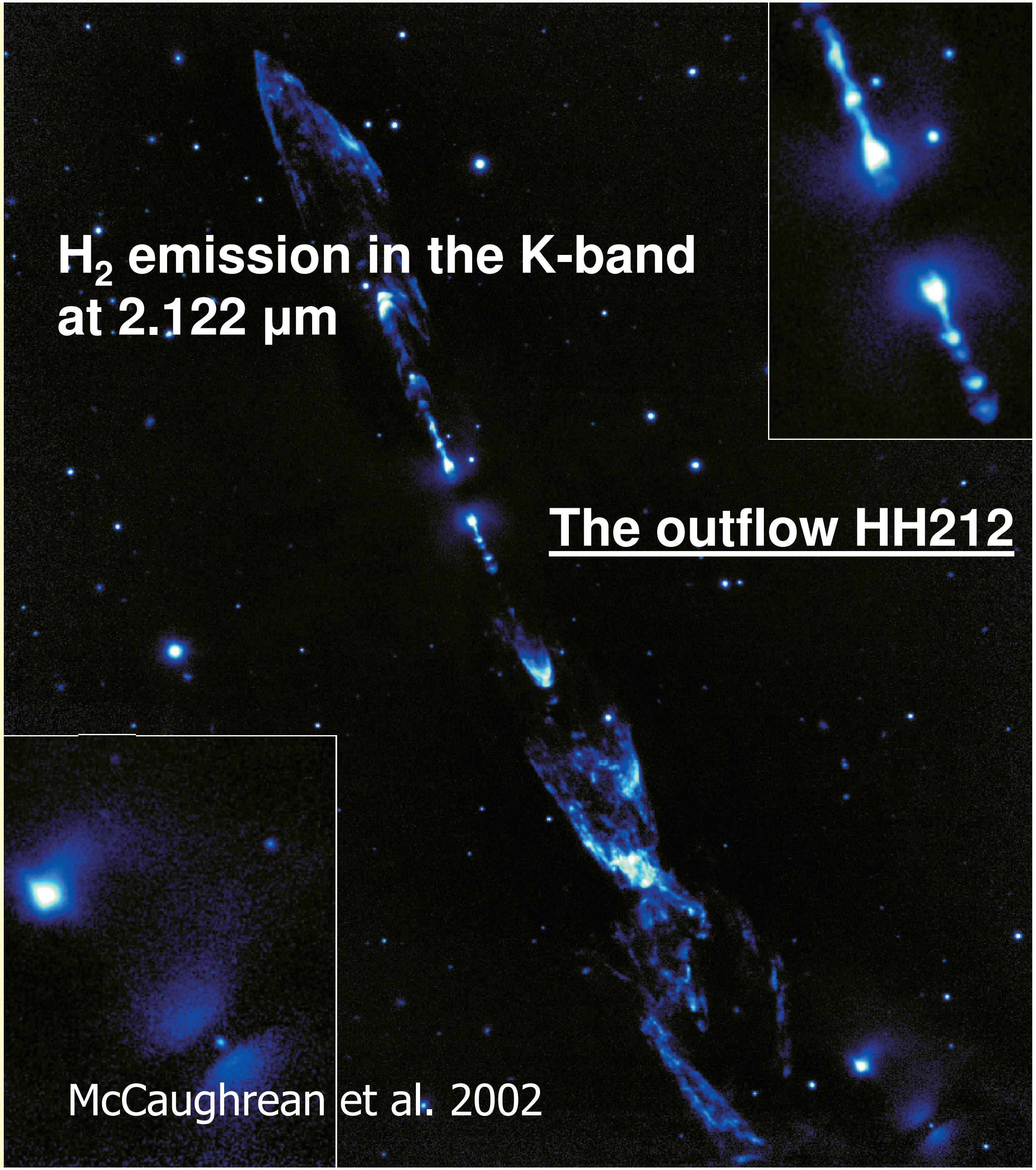

H_2 emission in the K-band
at 2.122 μm
The outflow HH212
McCaughrean et al. 2002

Hot-spot observations

Image of the HH47A bow-shock (Hartigan et al. 1999)

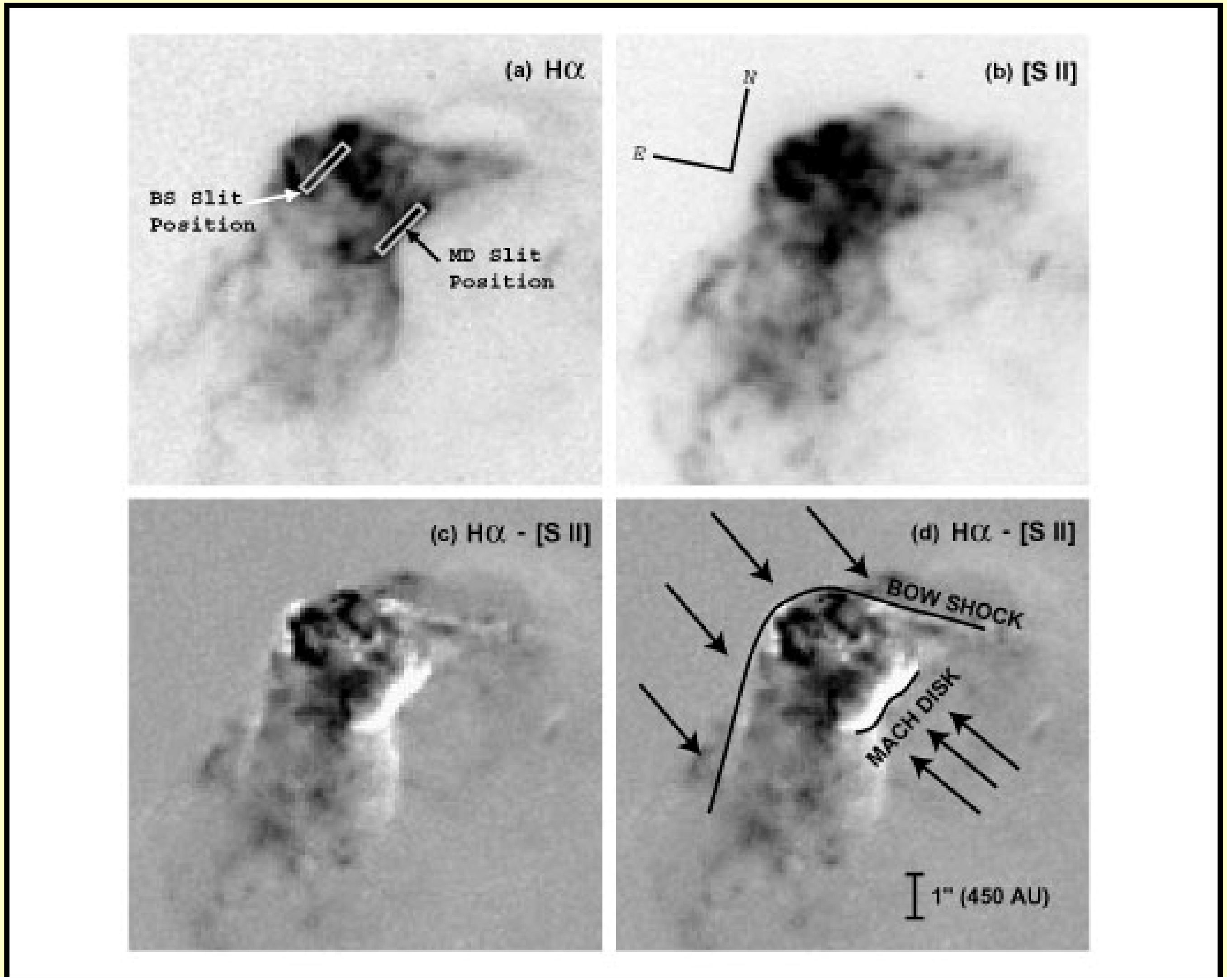

Hot-spot observations

HH47A bow-shock spectrum

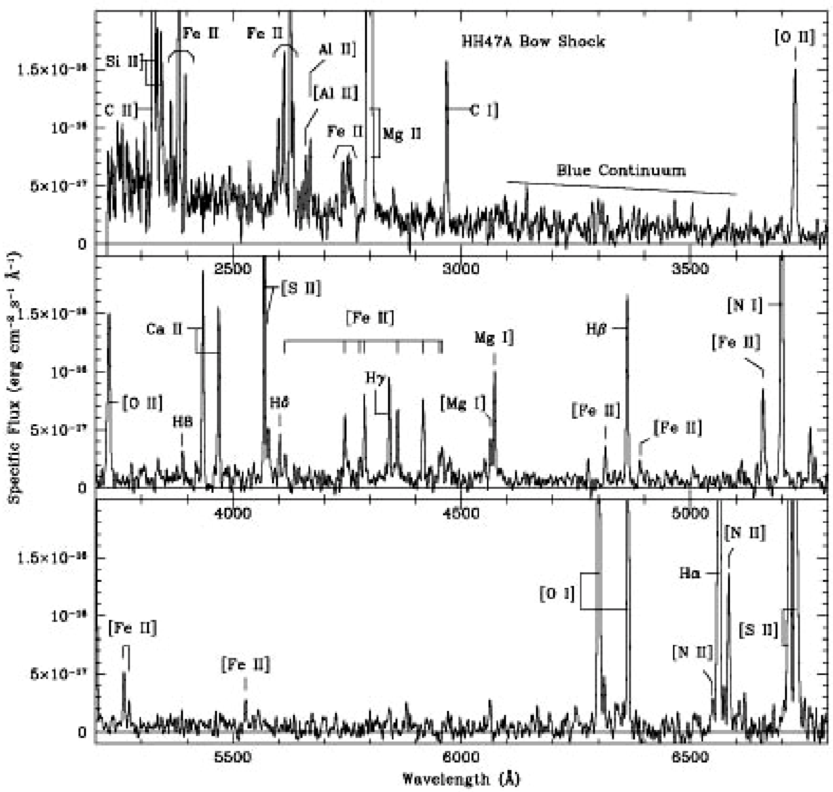

HH47A Mach-disk spectrum

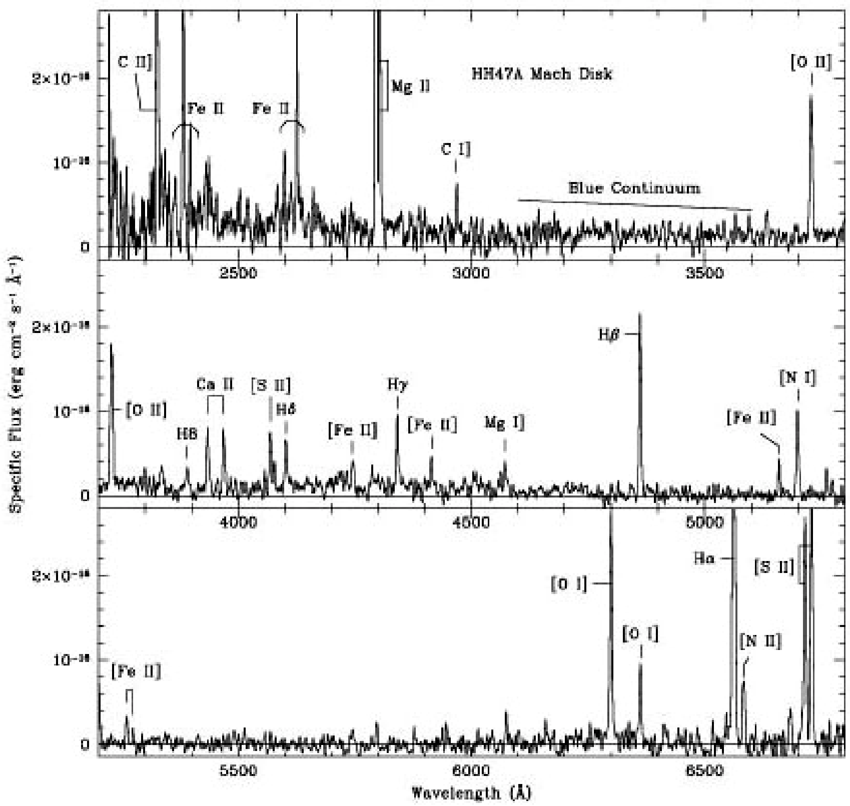

Hot-spot observations

Constraints on physical parameters:

$$\frac{\text{[S II] } 6716}{\text{[S II] } 6731} \longrightarrow \boxed{N_e} \qquad \frac{\text{[O III] } 5007 + \text{[O III] } 4949}{\text{[O III] } 4363} \longrightarrow \boxed{T}$$

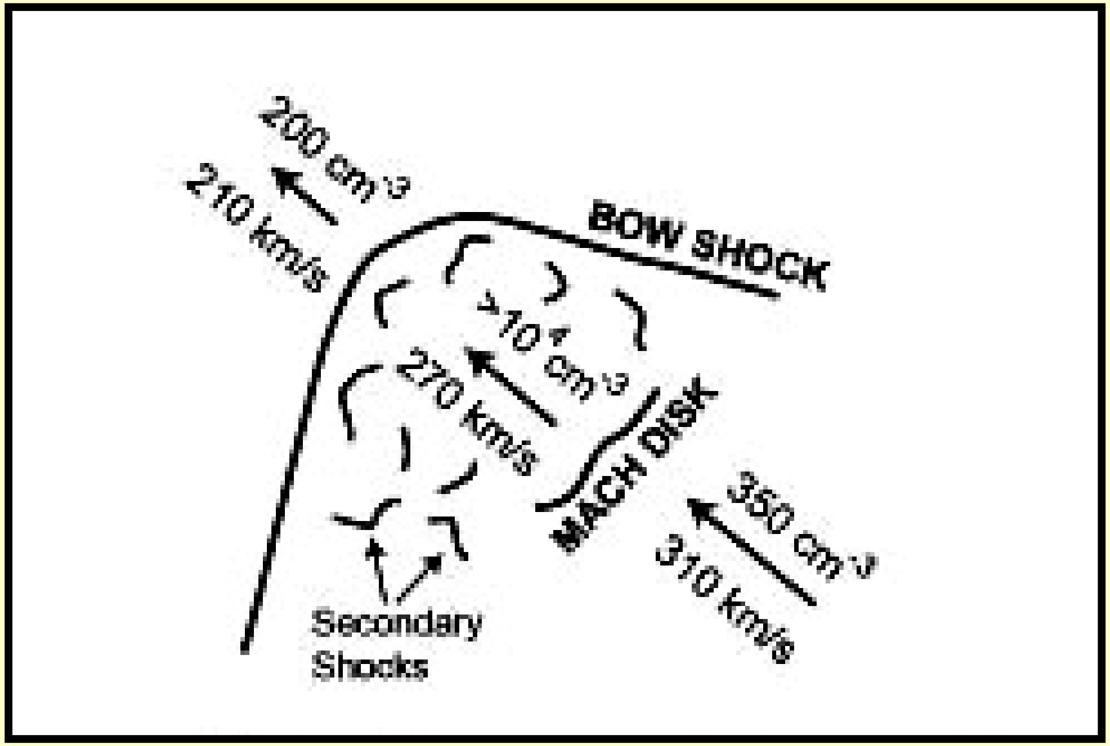

Jet morphologies

HH212 - IR

The medium surrounding the jet is not observable at any wavelength

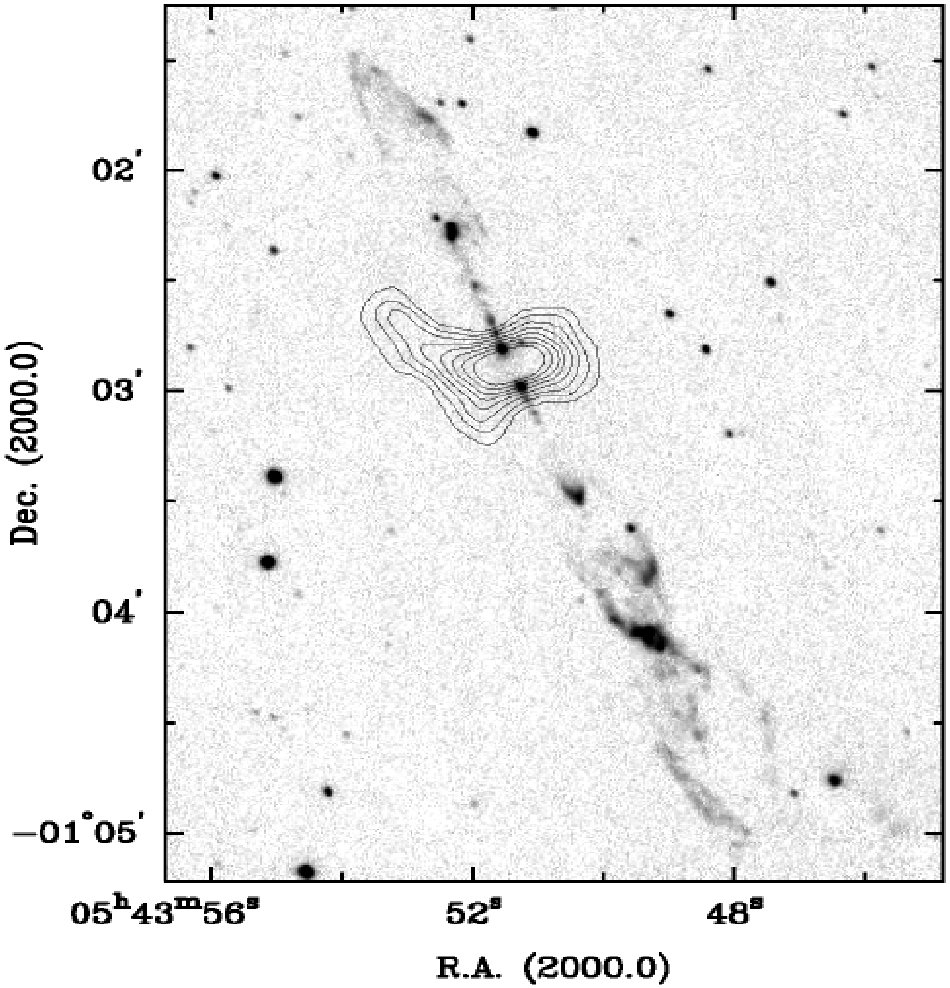

1. **Jets with little evidence of cocoons**
2. **Jet one-sidedness from ambient absorption**

From morphologies

YSO jets are as dense as the ambient (or denser)

Jet morphologies

Comparison with a "classical double" radio source:

Prominent cocoon ⟶ underdense jets

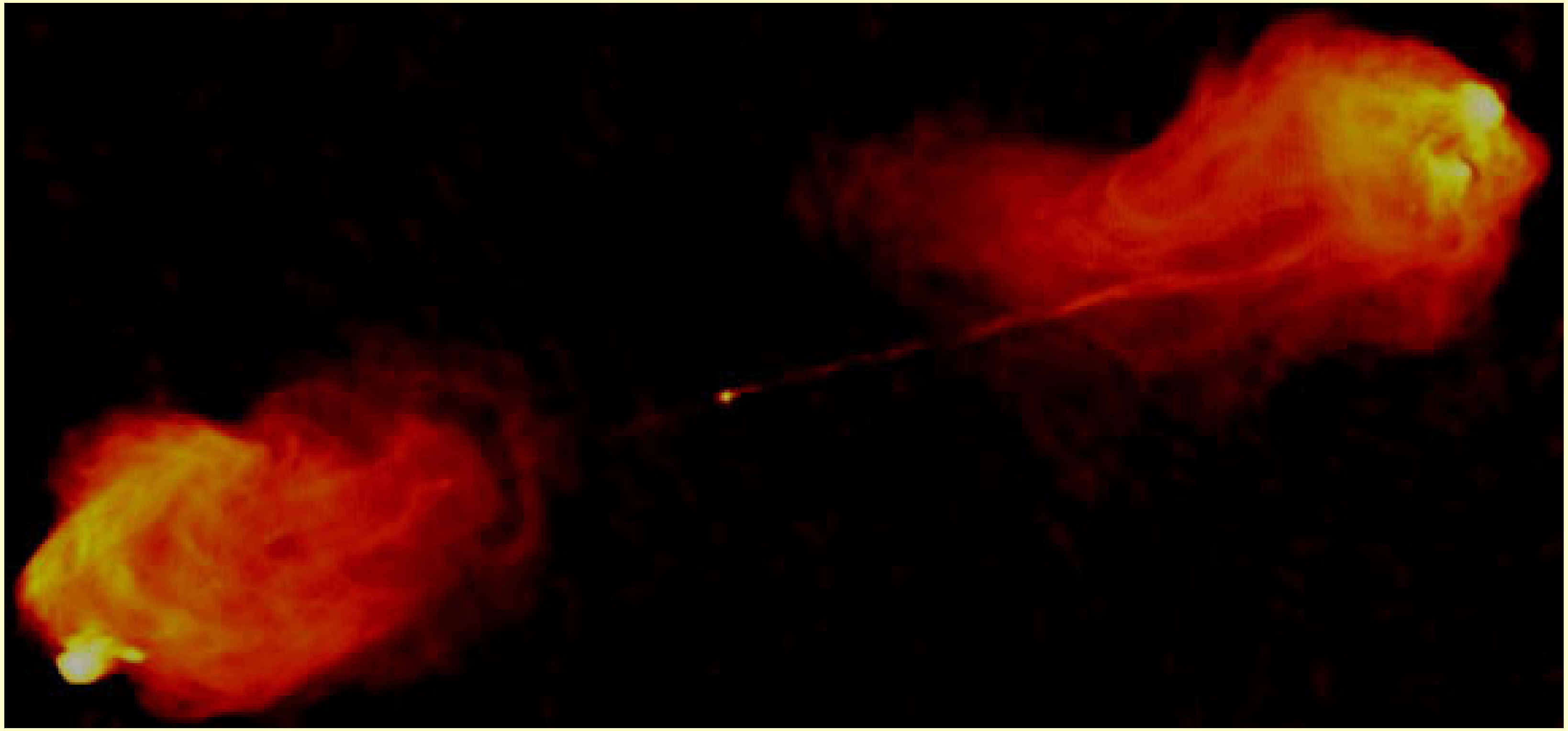

YSO Jets: Large scale knots

HH34 optical

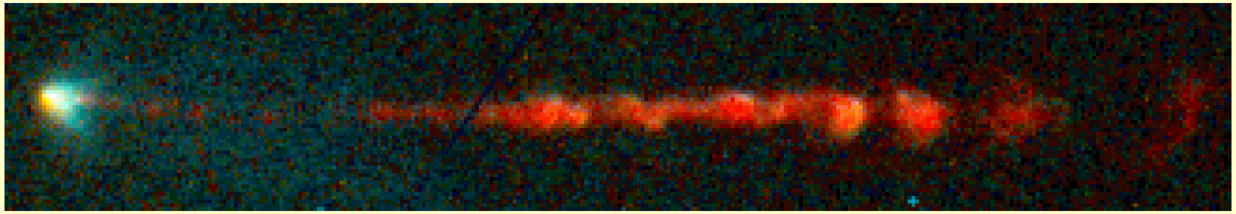

HH34 optical

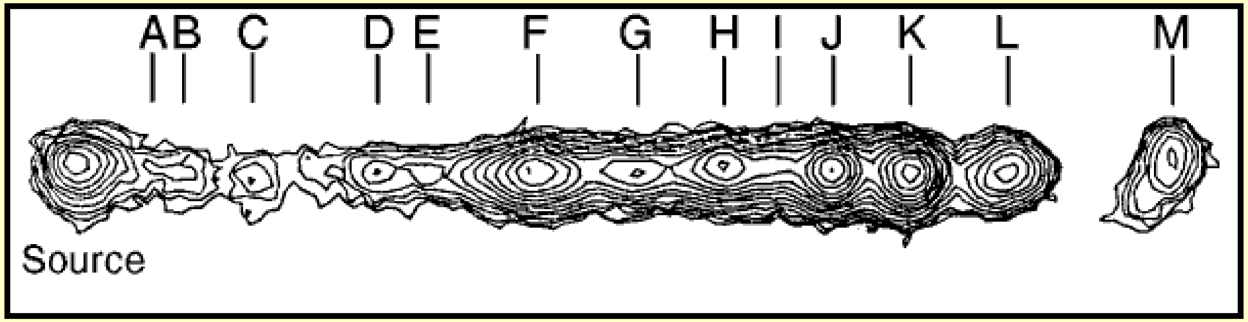

3C 273 Radio+ optical

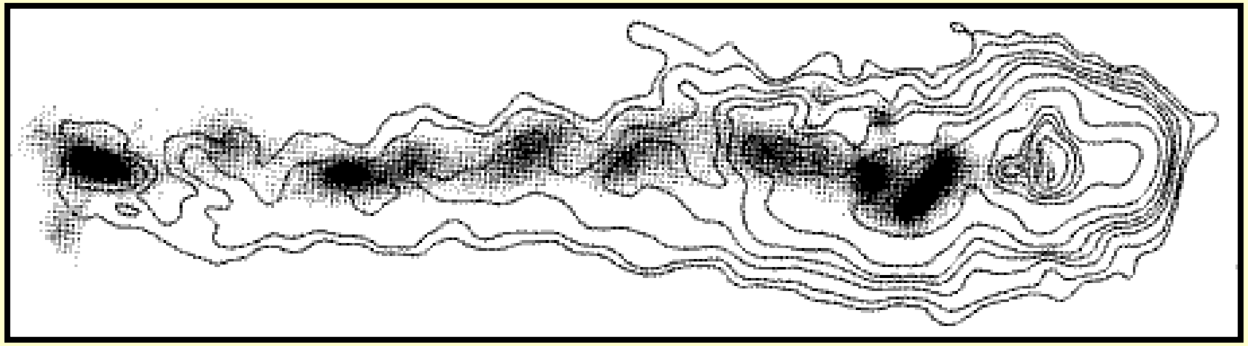

YSO Jets: Large scale knots

HH34: Proper motions
(Eislöffel & Mundt 1992)

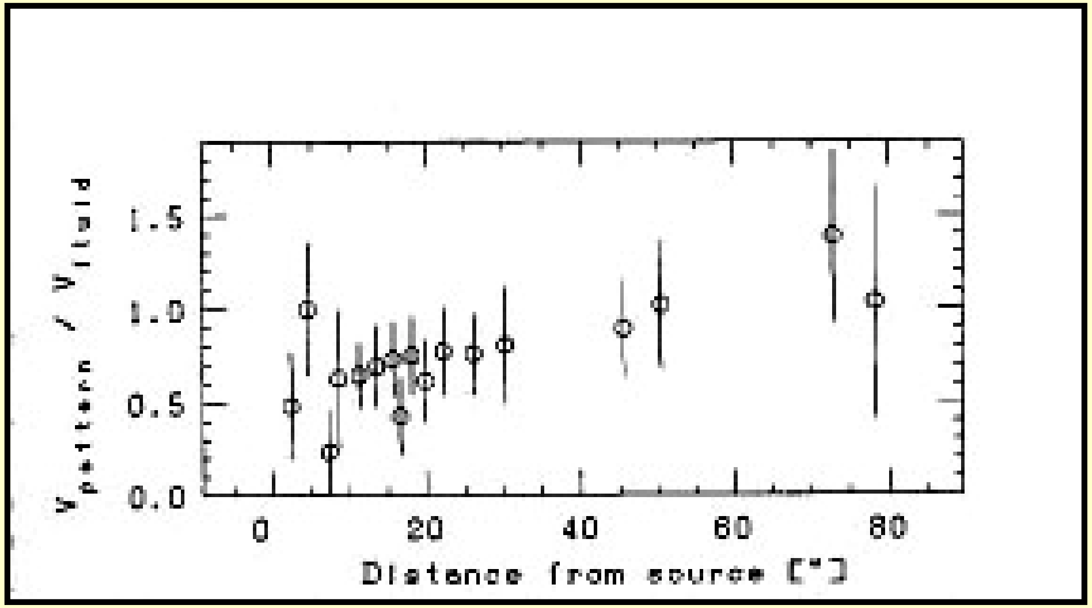

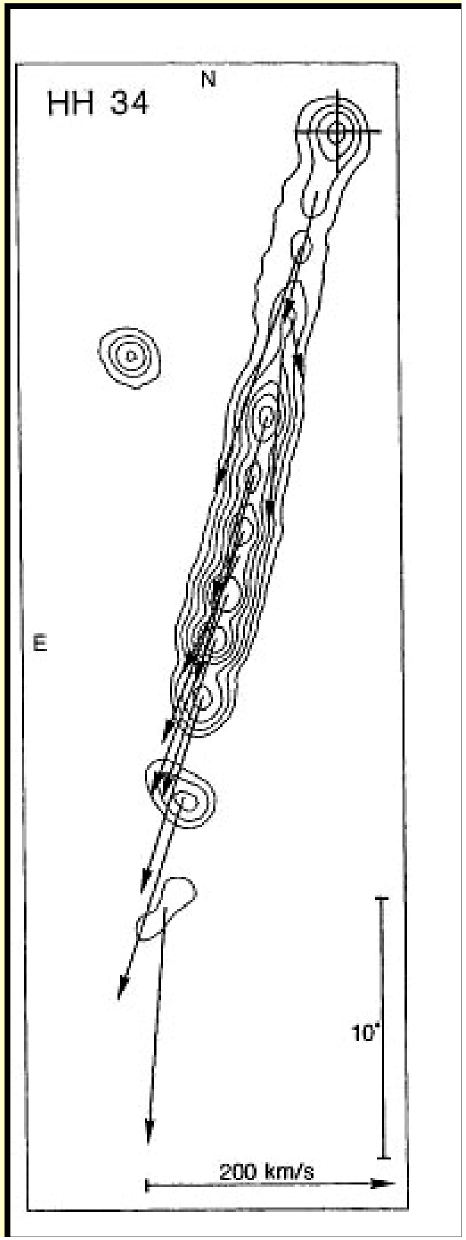

Summary of YSO jets physical parameters

Forbidden emission line ratios → electron densities, temperatures

Line Doppler shifts → jet radial velocities

Knot proper motions → tangential velocities

Jet kinetic power (ergs s^{-1})	10^{30-33}
Jet length (pc)	$\gtrsim 1$
Jet's diameter ($\times 10^{14}$ cm)	$\sim 1-10$
Age (yr)	$\gtrsim 10^4$
Electron density (cm^{-3})	$\sim 10^3 - 10^4$
Ionization fraction	2-30 %
Temperature (K)	$10^3 - 10^4$
Jet velocity (km s^{-1})	200 - 400
Jet Mach number	20 - 40

Ray et al. (1996), Reipurth & Bally (2001), Bacciotti & Eislöffel (1999)

YSO Jets: Large scale knots

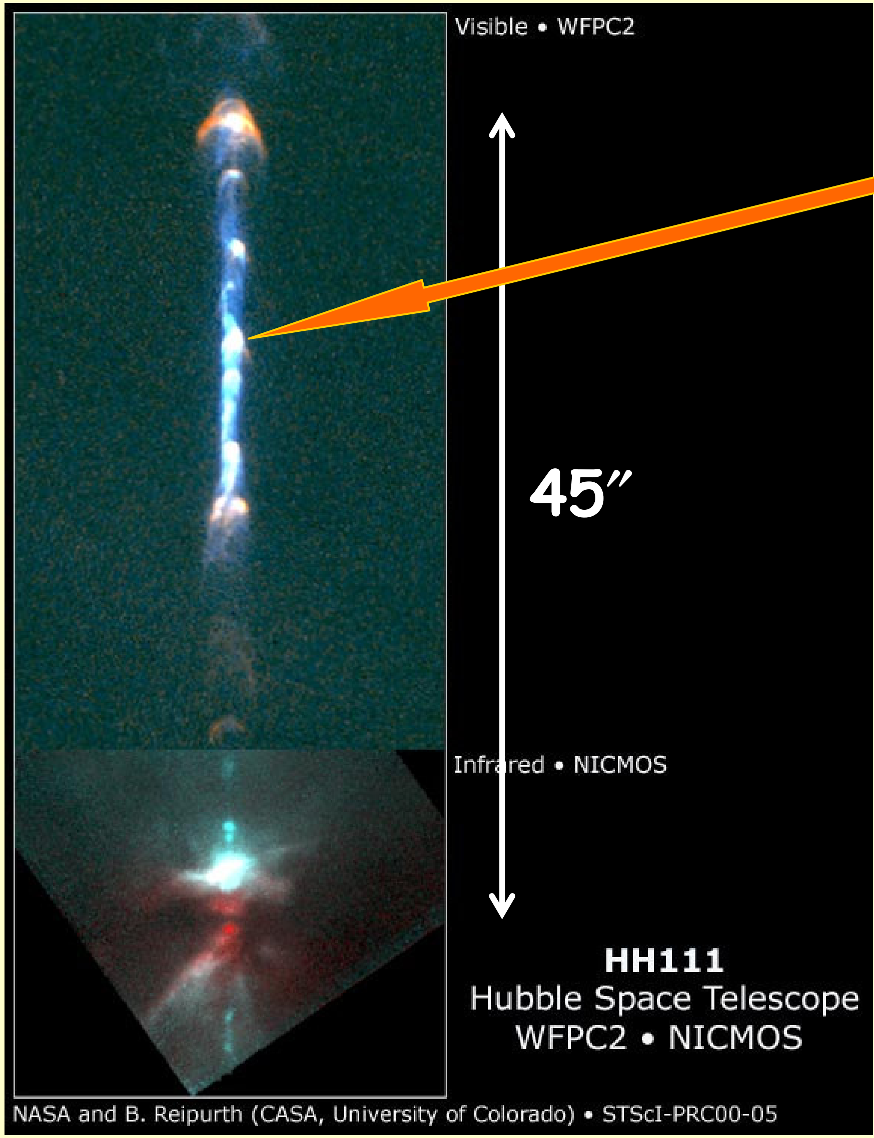

Knots due to:

1) **Internal Working Surfaces?**
2) **Shear-layer Instabilities?**
3) **Current-driven modes**
4) **Re-collimation shocks?**

YSO Jets: Small scale knots

Distances $\lesssim$ 5''

RW AUR Jet
([S II] and [O I])

Dougados et al. 2000)

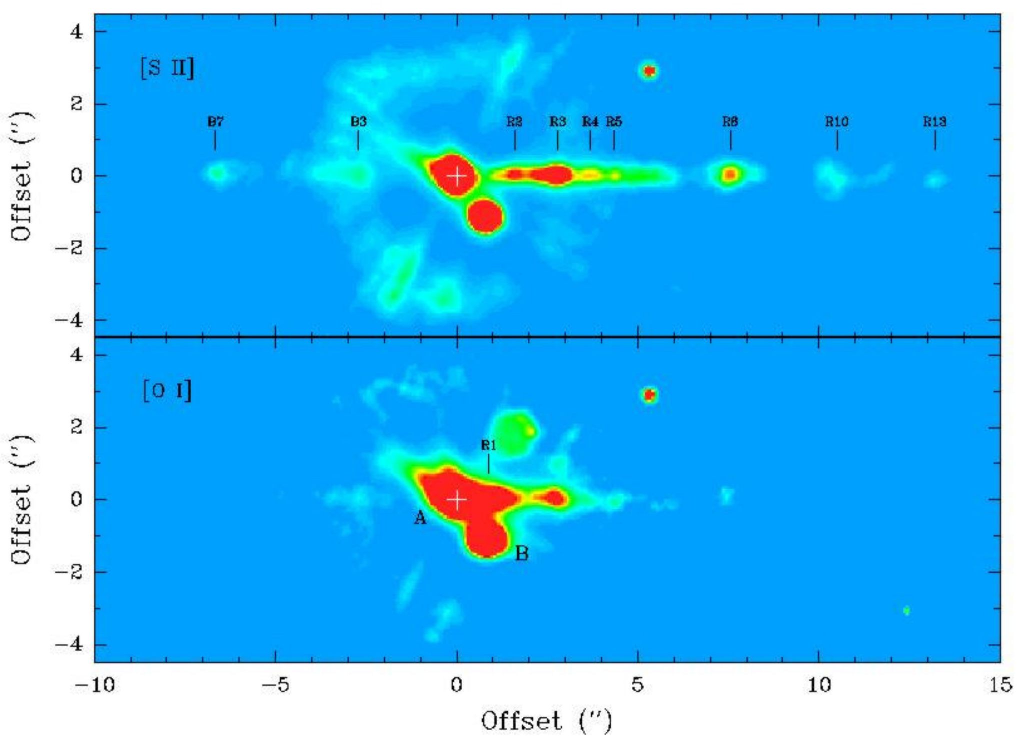

DG TAU B jet
(continuum)

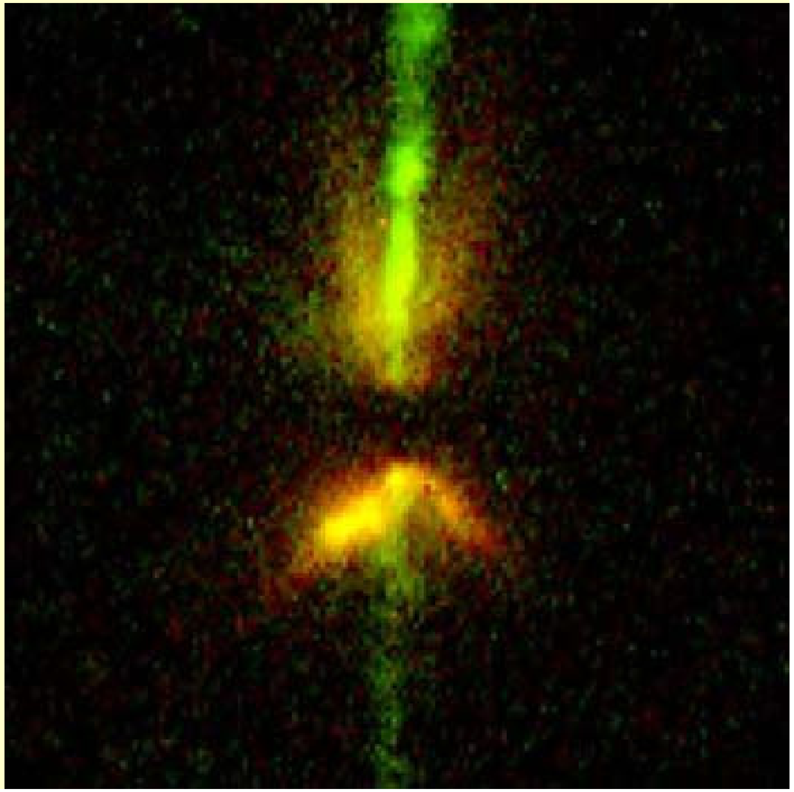

Simulated cooling jet

HH30 jet

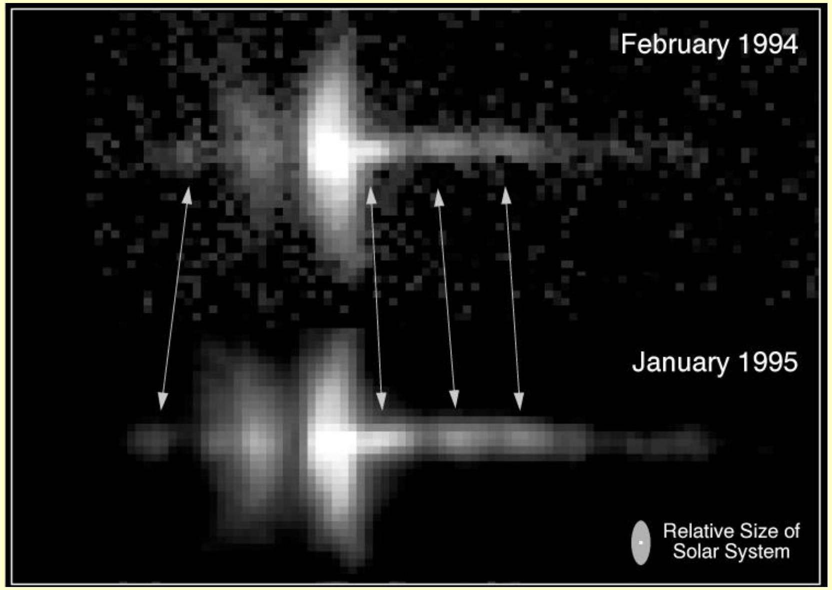

V_j=200 km s^{-1}, n_j/n_{amb}=1, p_j/p_{amb}=10

Species: H, He^0, C^0, C^+, N^0, N^+, O^0, O^+, Mg^+, Si^+, S^+, Fe^+

HH30 (Bacciotti et al. 1999)

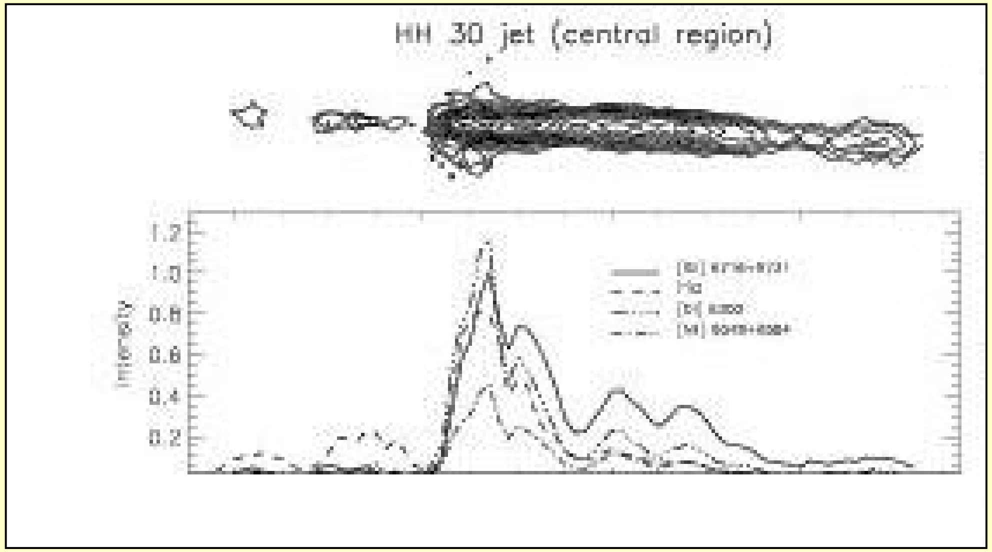

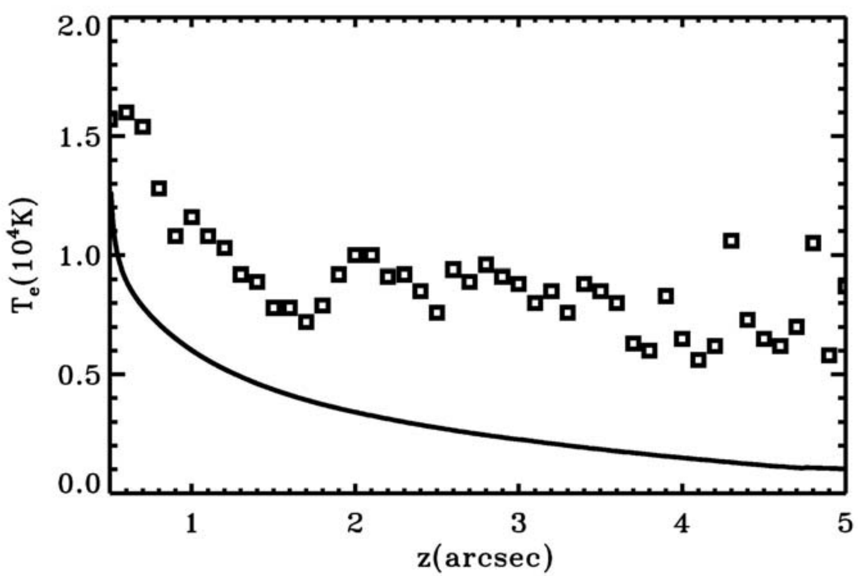

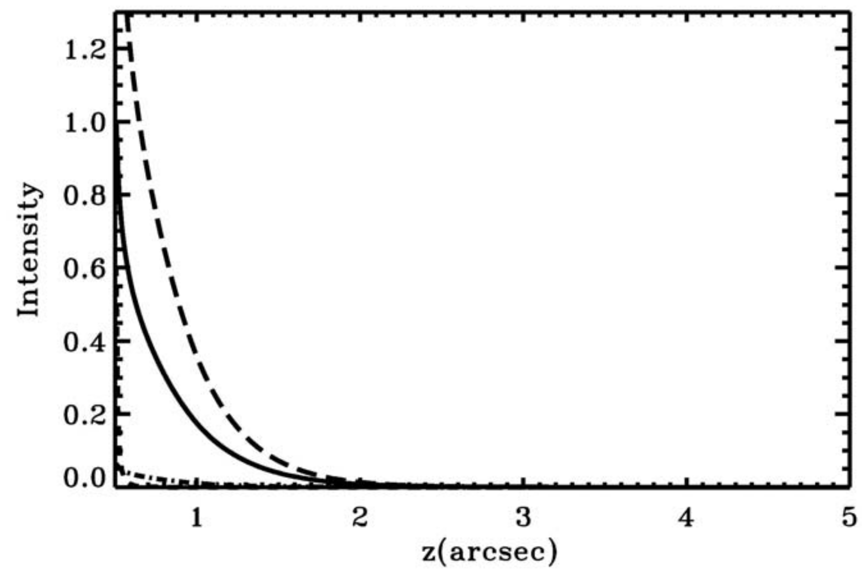

Shock excitation

One observes post-shock regions of higher excitation (*filling factor <<1*, Hartigan 2004)

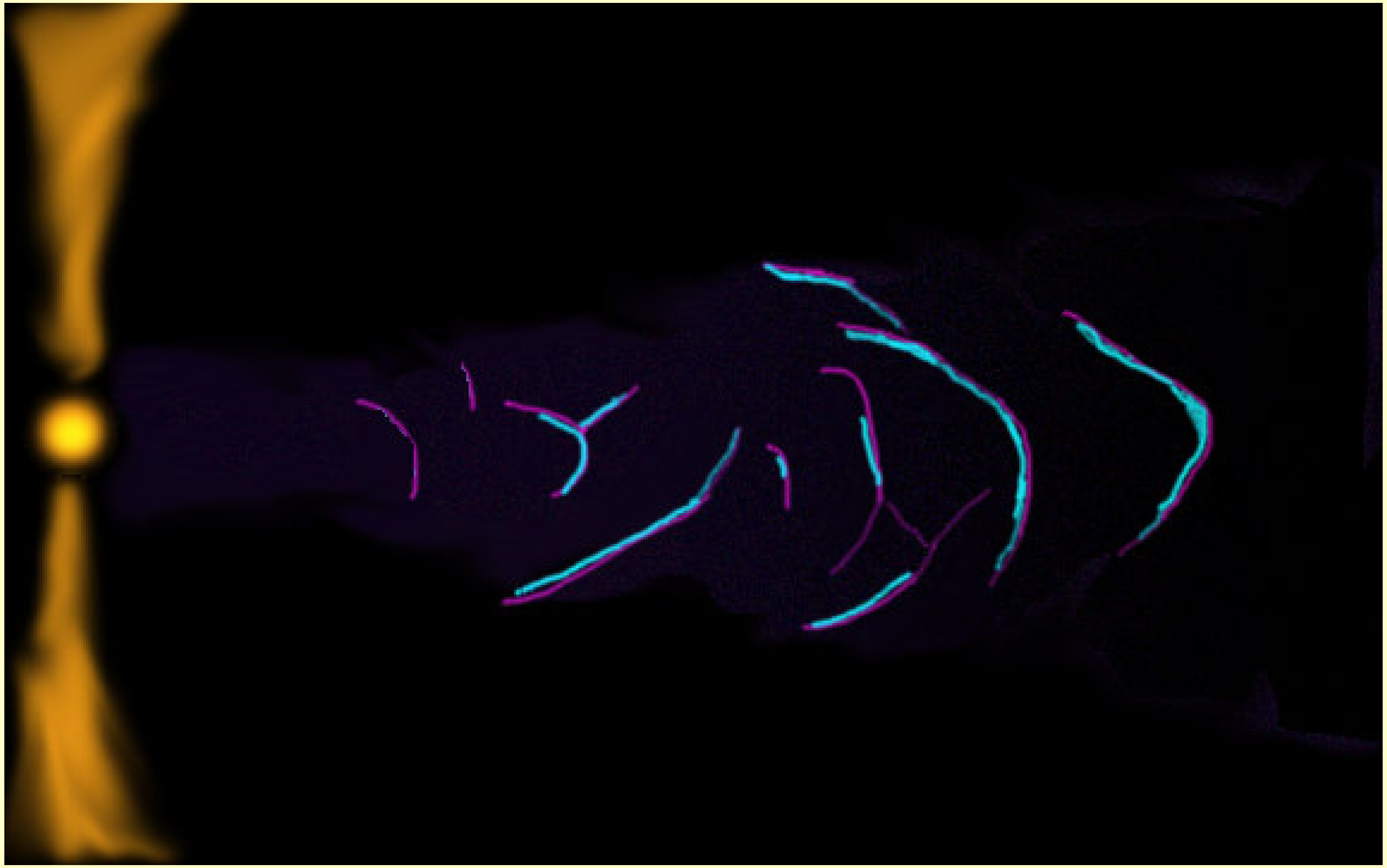

Shock excitation

Temporal evolution of a velocity perturbation

Density and velocity at different times in the reference frame at rest with the mean flow of the jet

Perturbation amplitude: U_0=70 km s^{-1}

Preshock parameters:

T_{up}=1000 K, $n_{up}=n_0\, x_0^2/(x_0^2+x^2)$, x_0=0.1

$n_0=5\times10^4$ cm^{-3}, B_{up}=100 μG, $f_{i\ up}$=0.1%

Massaglia et al. (2005)

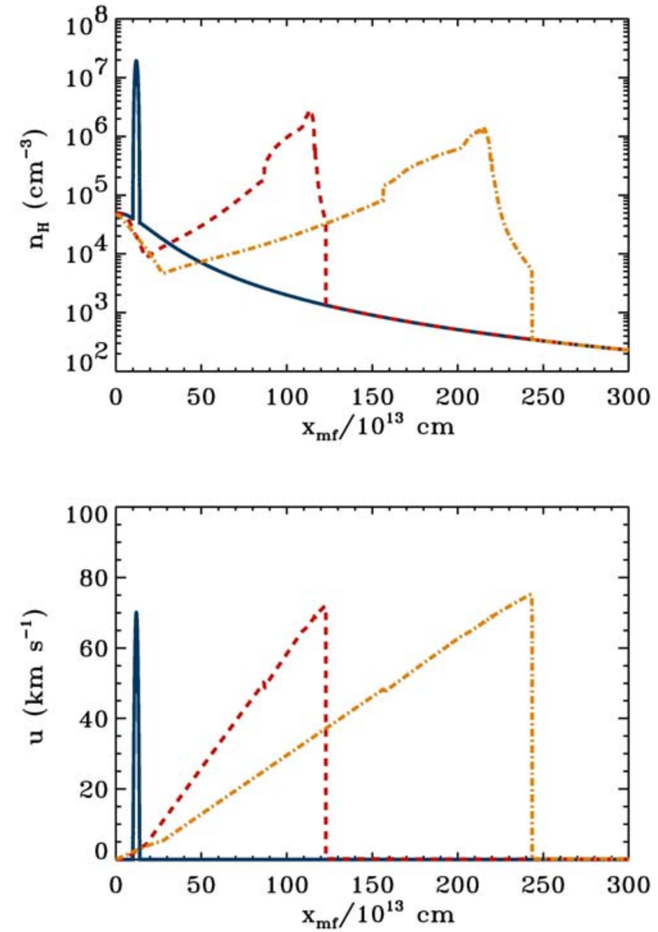

Line-ratios along the jet

Comparison of observations (C. Lavalley-Fouquet et al. (2000), symbols) with the model (Massaglia et al (2005), lines)

(*,◇) = Log[SII] and Log[NII/OI] ratios from

C. Lavalley-Fouquet et al. (2000)

DG Tau jet assuming advection velocity V_{flow}=150 km s^{-1}

(°)=electron density from [SII] ratio

(•)=Ionization fraction (Bacciotti et al. 1995)

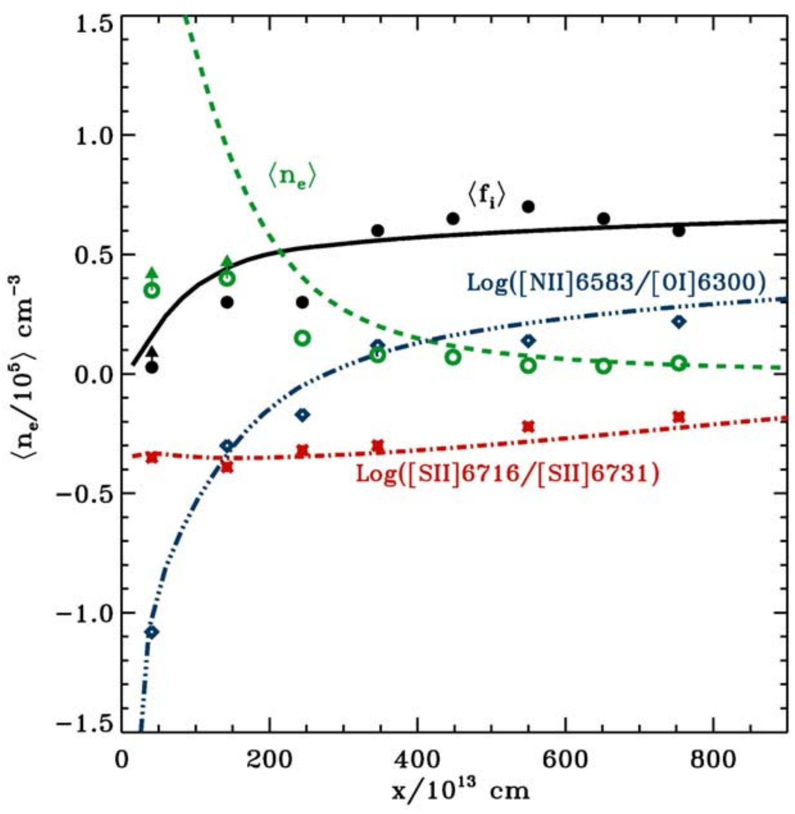

Modelling the origin of jets

Jets originate around SMBH of 10^8-10^{10} $M_\odot$ accreting mass through a magnetized disk

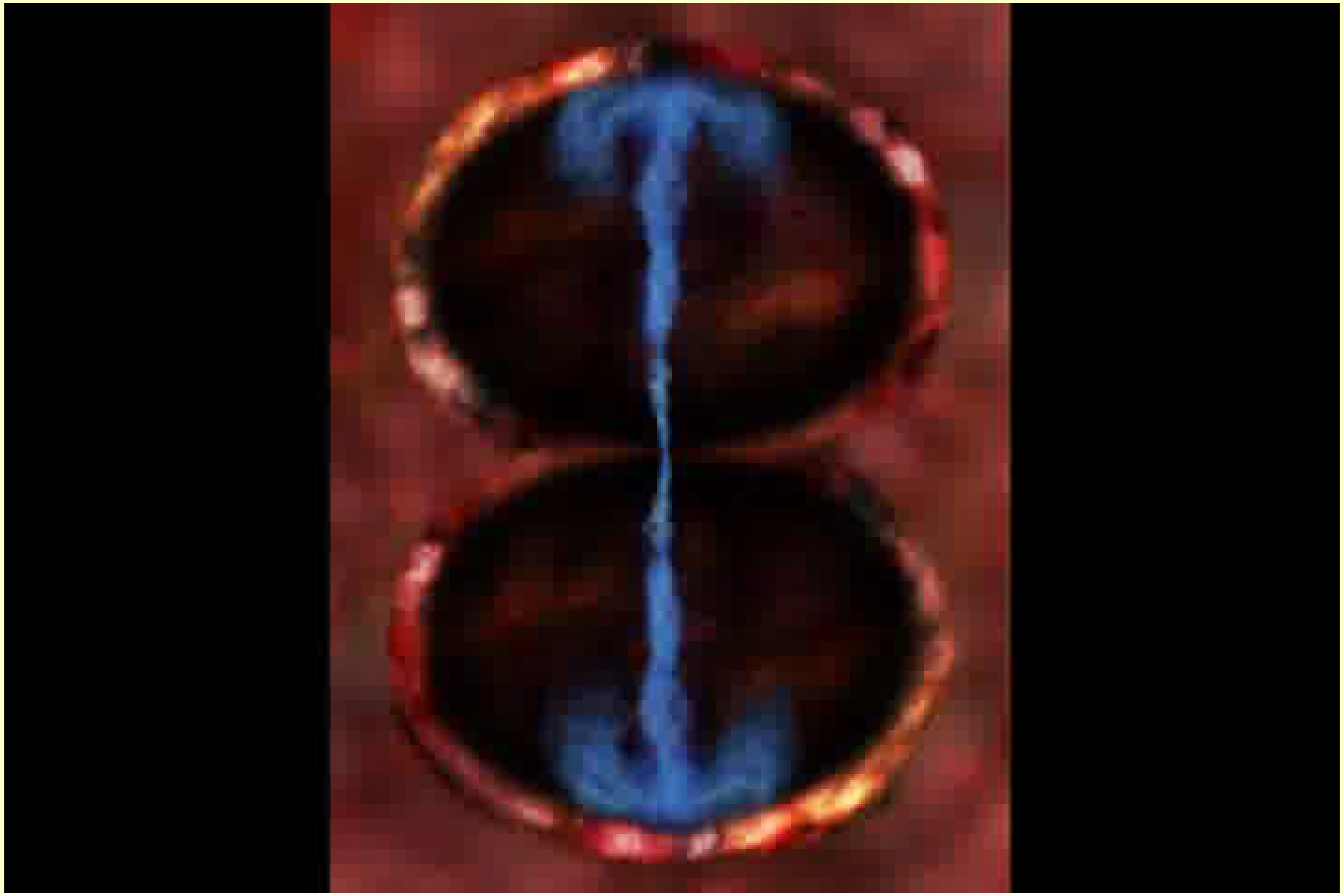

Jet acceleration: classes of models

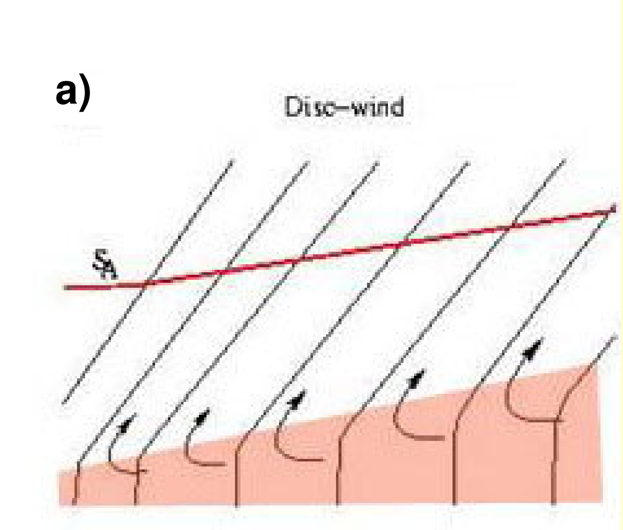

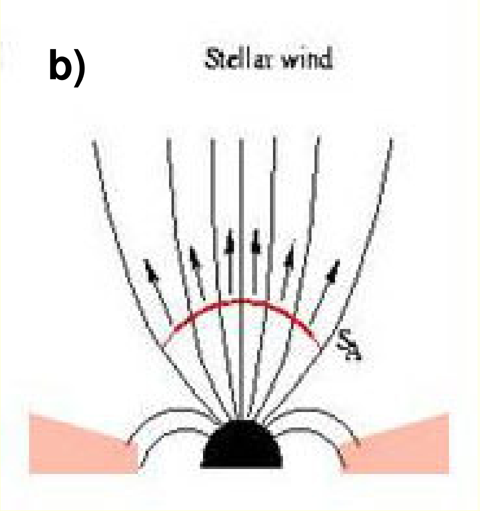

a) **Disk-wind models**
   acceleration: centrifugal below the alfvènic surface, magnetic pressure gradient above
   collimation: magnetic tension (hoop-stress)

b) **Stellar wind models**
   acceleration: mostly due to pressure gradient
   collimation: magnetic tension

Disk-wind jets: stationary models

Blandford & Payne (1982), Camenzind (1996)
Spruit (1996), Ferreira (1997)
Vlahakis et al. (2000)

No corotation

Corotation

Thin disk

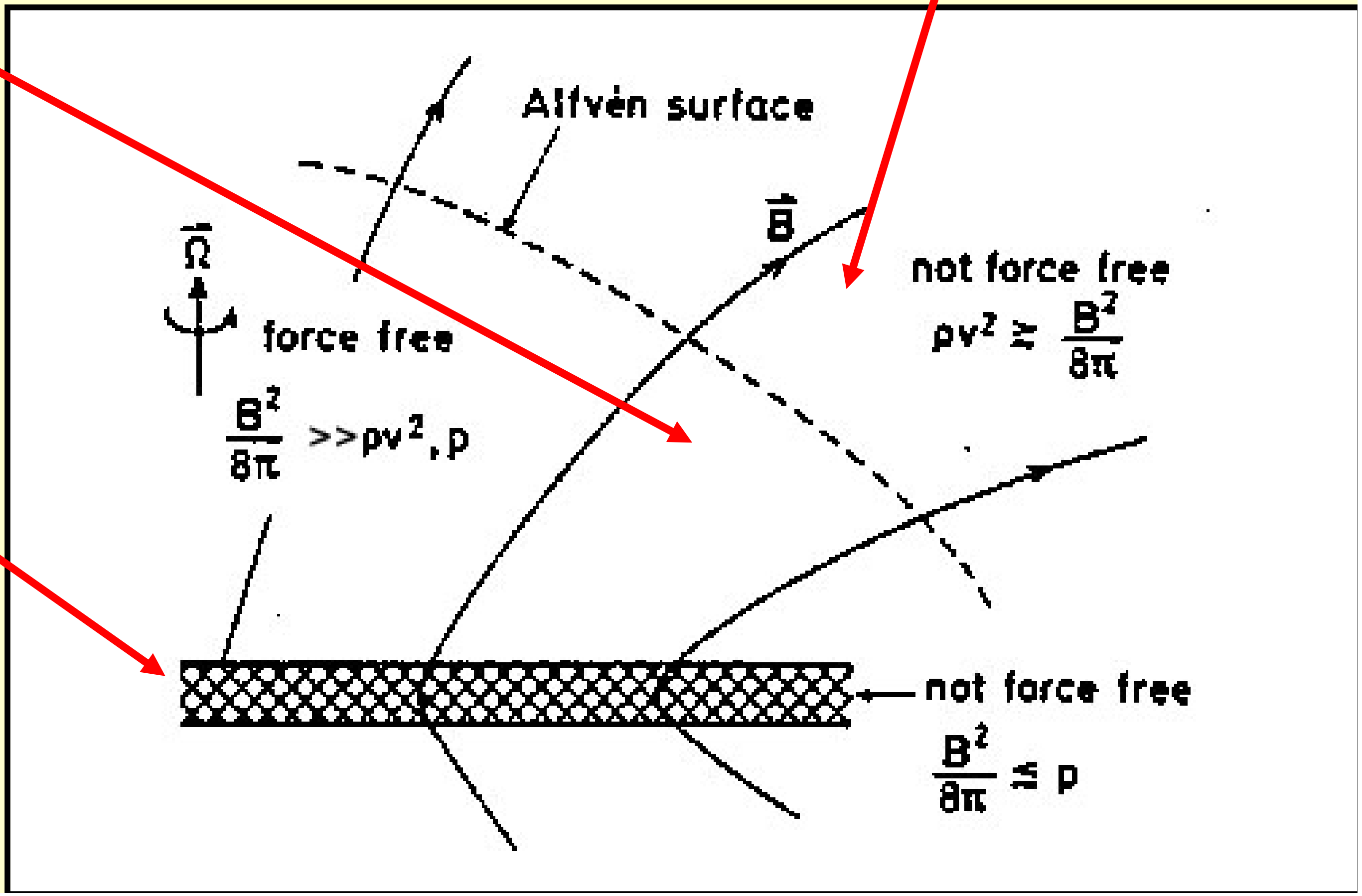

DW jets: launching mechanism

1. Θ > 60°: no flow
2. Θ ≤ 60°: wind
3. Θ << 60°: slow flow

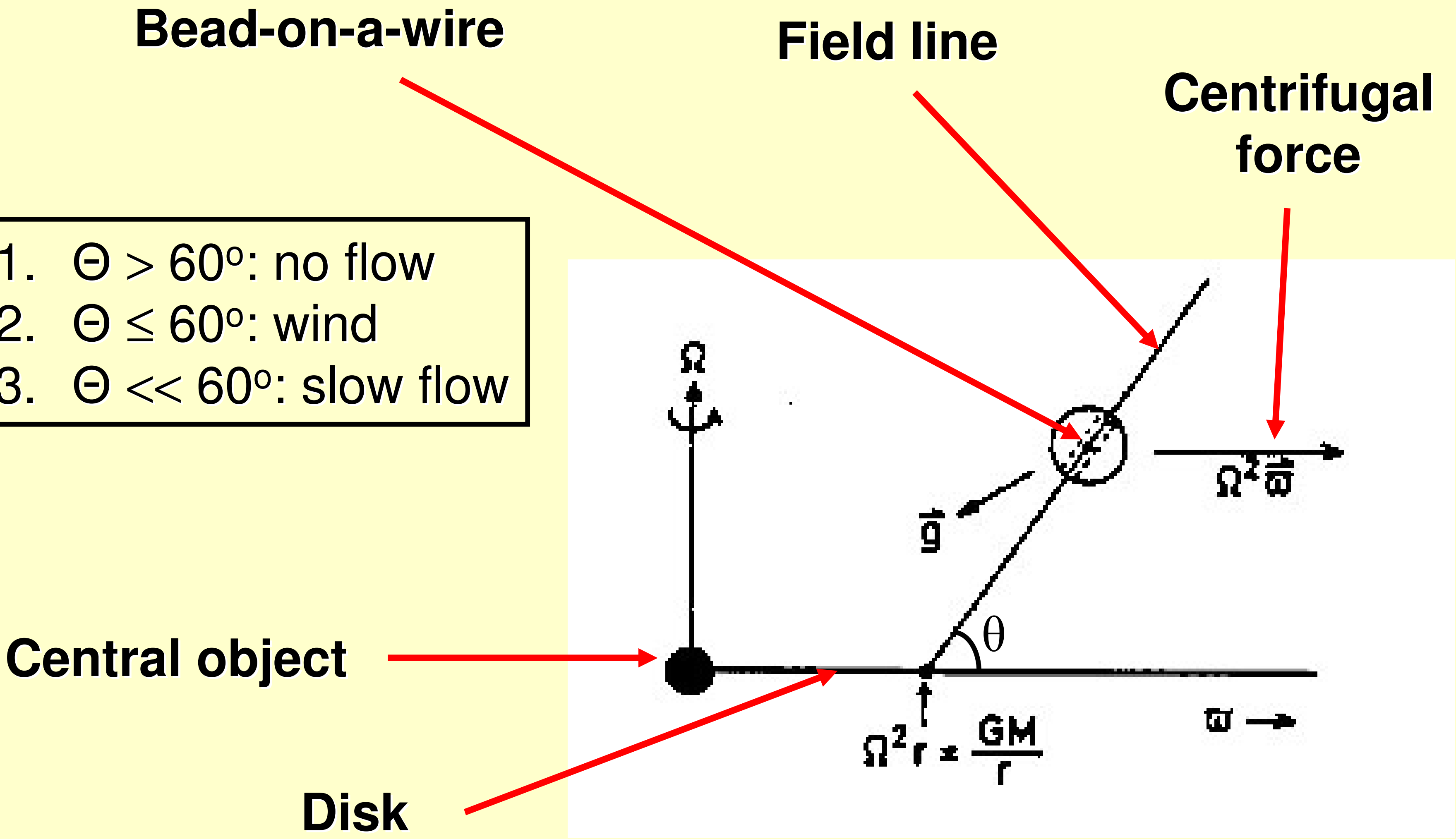

DW jets: launching mechanism

Collimation:
Magnetic tension
(Hoop-stress)

Acceleration:
Magnetic pressure
gradient

Acceleration:
centrifugal

Central object

Disk

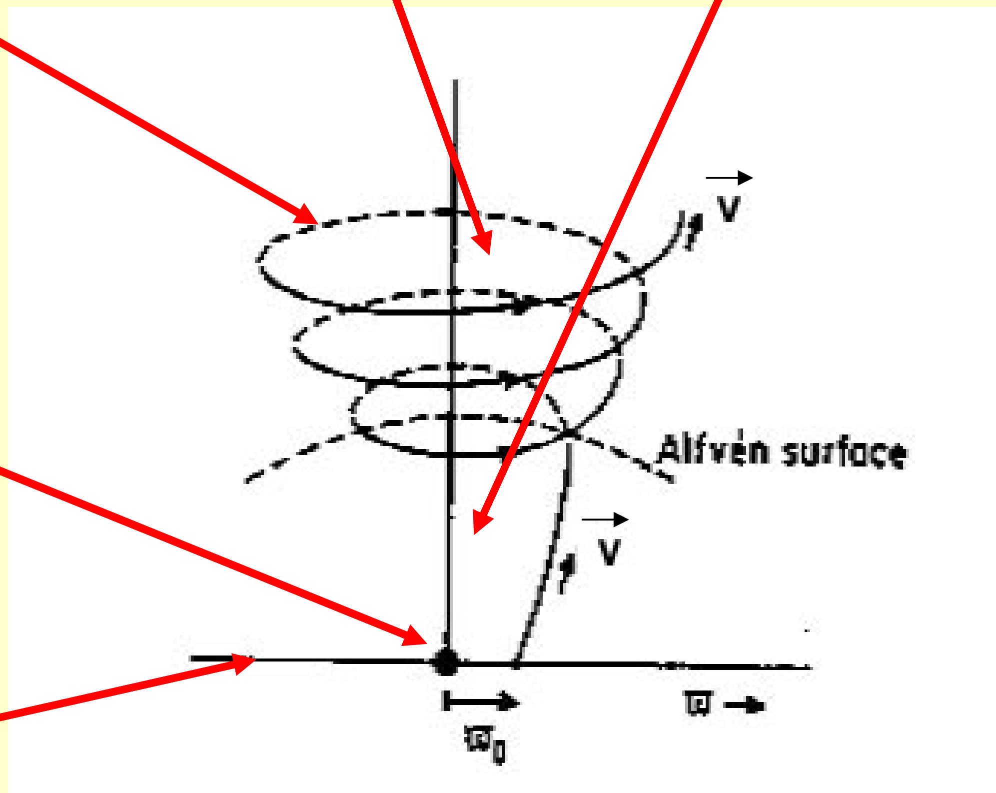

Analytical Approaches

- **The ideal, steady-state axisymmetric MHD equations have been solved by a non-linear separation of the variables**
- **Solutions are obtained by the assumption of self-similarity, which implies the invariance along one direction of the spherical coordinates (r, θ)**
- **The analytical models provide density and the velocity and magnetic field vectors as functions of (r, θ)**

  – Radially Self-Similar (a) ϖ_1 / ϖ_2 the same for any θ

  – Meridionally Self-Similar (b) ϖ_1 / ϖ_2 the same for spherical surfaces

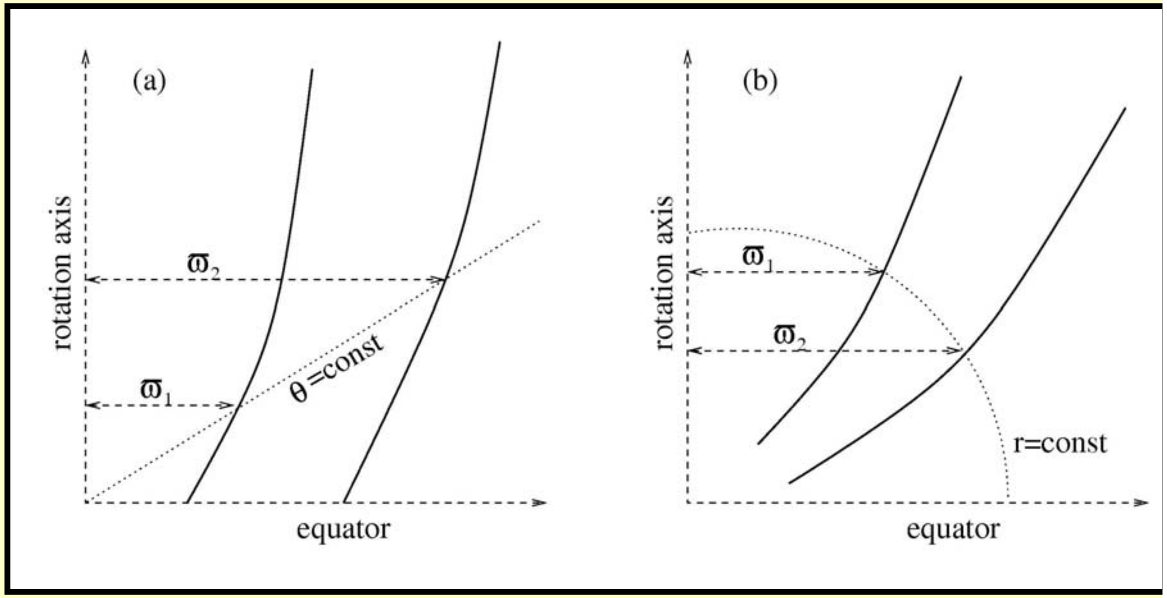

The solutions

The Radially Self Similar Models:

- describe a magneto-centrifugally disk wind
- they have conical critical surfaces (slow, Alfvèn, fast)
- however, they are singular at the axis
- they are derived with the polytropic assumption with a constant polytropic index

(Contopulos & Lovelace 1994, Ferreira 1997, **Vlahakis et al. 2000**)

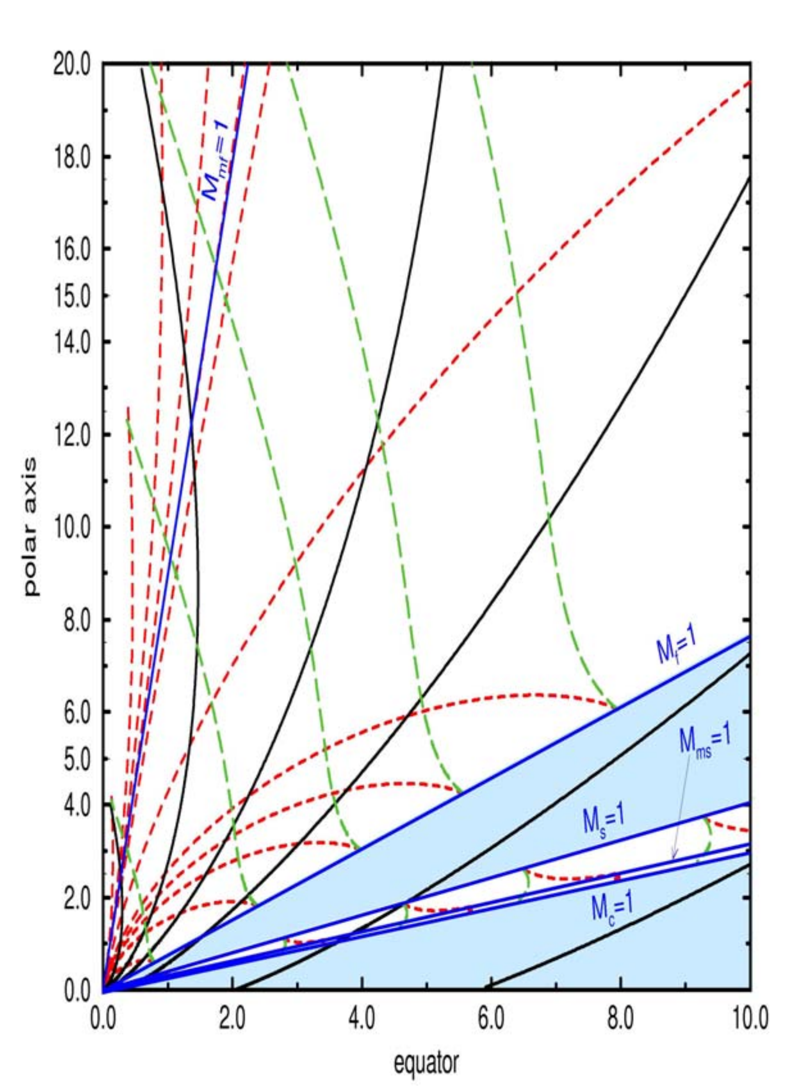

The solutions

Meridionally Self Similar Models:

– describe a thermally driven stellar outflow
– have spherical critical surfaces (slow, Alfvèn, fast)
– there are magnetic fieldlines not connected to the star surface
– they correspond to a variable effective polytropic index

(Sauty & Tsinganos 1994, Trussoni et al. 1997, **Sauty et al. 2002**)

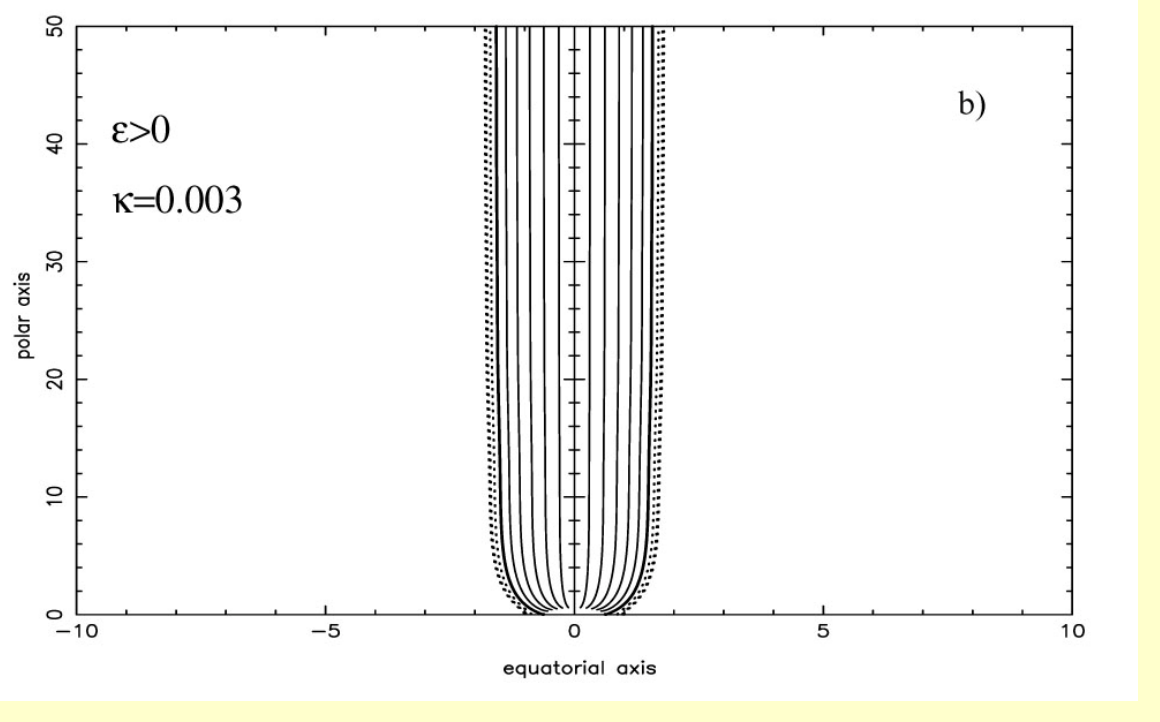

Numerical simulations

MHD jet acceleration studies by numerical means,
in 2D axisymmetry:

1. Considering the disk as a given boundary condition (e.g., Ouyed & Pudritz 1997, Ustyugova et al. 1999, Fendt 2006);
2. Producing accretion-ejection flows evolving disk and jet self-consistently (e.g., Casse & Keppens 2002, Kato et al. 2002, Zanni et al. 2007)

Accretion-ejection: initial setup

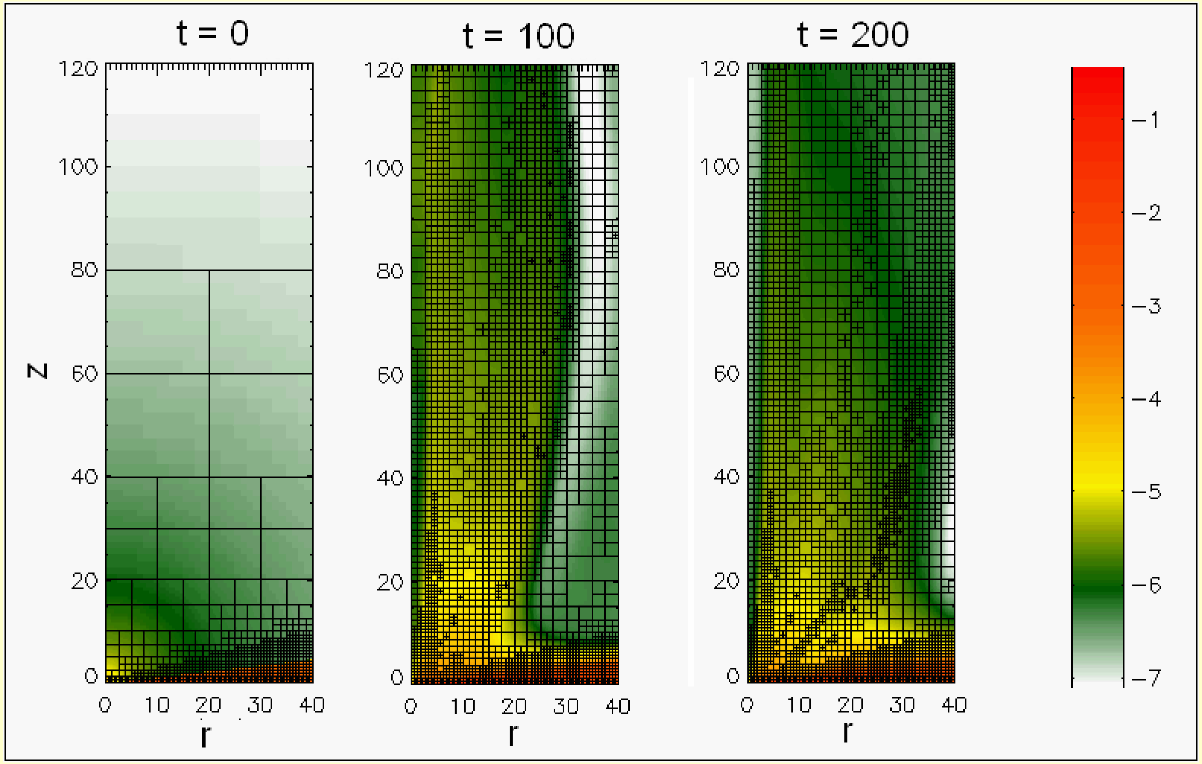

2.5D MHD

FLASH2.5 – AMR

7 levels of refinement

512x1536
([illegible]ivalent resolution)

Self-similar "Keplerian" disk in equilibrium with gravity, thermal pressure gradient and Lorentz force

Disk parameters: $\mu = B^2/P = 0.6$, $\eta = \alpha\, V_a\, H \exp[-2(z/H)^2]$

H=thermal disk heightscale=$(C_s/\Omega_K)_{z=0}$, η=magnetic diffusivity ("α" prescription)

Shakura & Sunyaev (1973), Ferreira (1997)

Time-dependent solutions

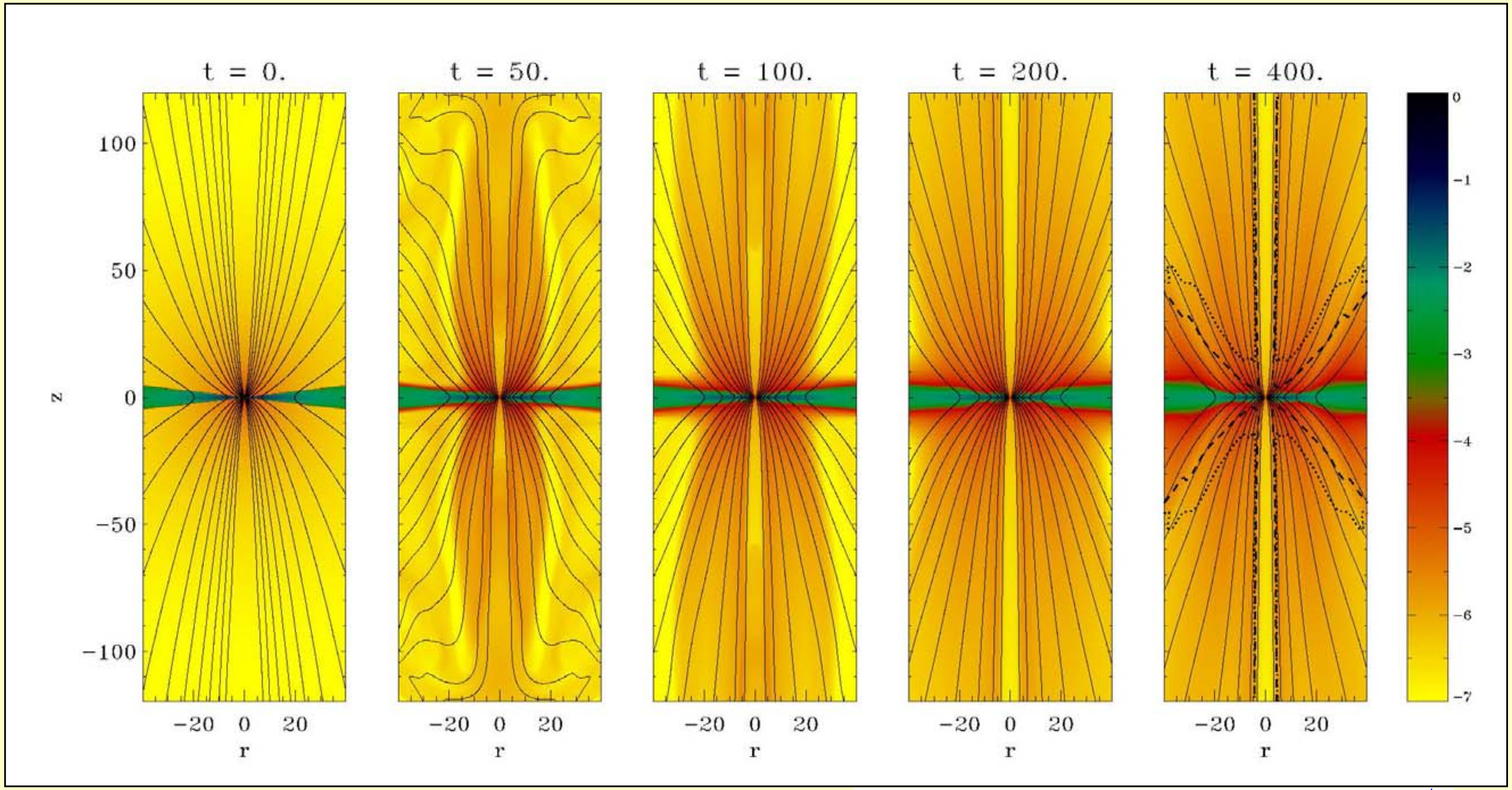

Density maps (logarithmic scale) Unit time: $t0 = r_0/V_{K0} = 1.7\,\frac{(r_0/0.1AU)^{3/2}}{(M/M_\odot)^{1/2}}$ days

Magnetic contour lines

Critical Alfvènic (dash), fast magnetosonic (dots) surfaces

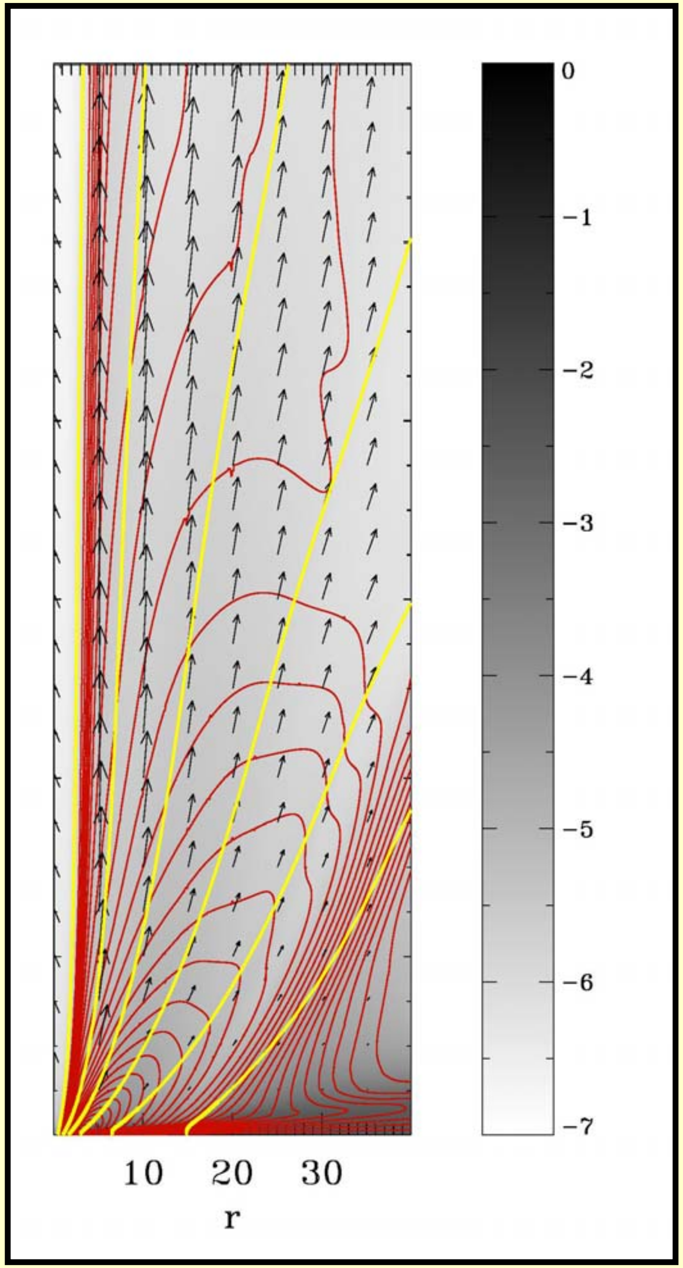

Poloidal current circuits (red)

Poloidal field lines (yellow)

Poloidal speed vectors

Background density gray-scale map (logarithmic)

Physical scales of the domain:

$z_{max} = 120\ r_0$
$r_{max} = 40\ r_0$

Mass loading – terminal speed

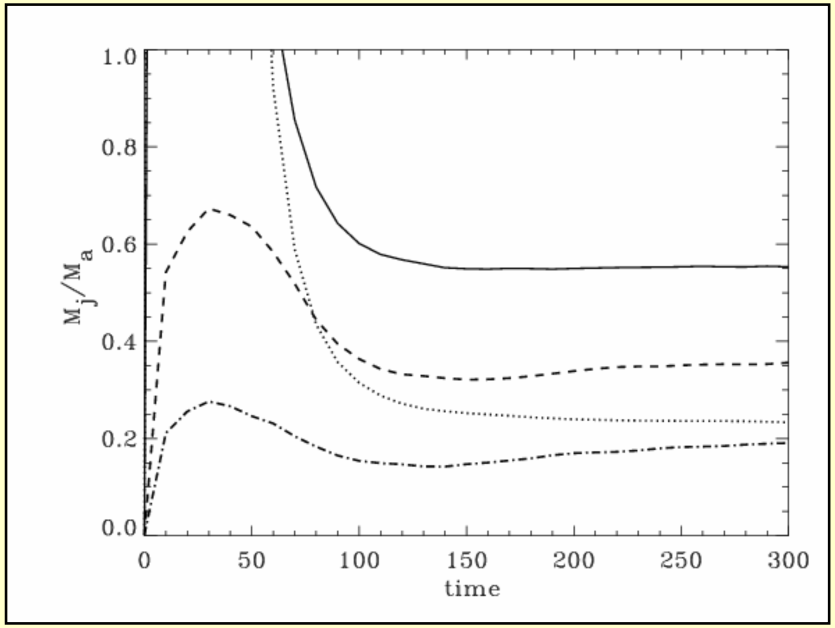

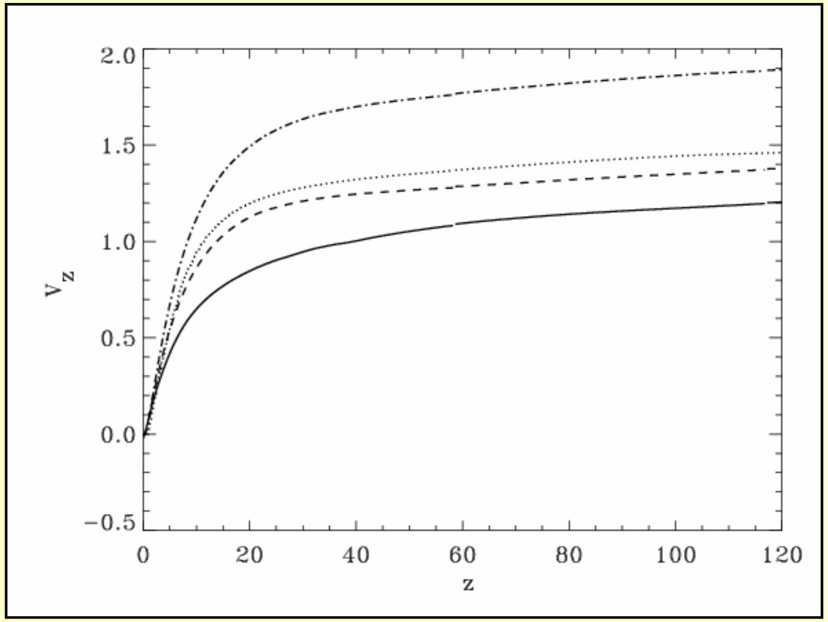

α = 0.1 χ_m=1

α = 1 χ_m=1

α = 1 χ_m= 3

α = 0.1 χ_m=1 low resolution

- More mass loaded outflows have lower terminal speed

➡ less available energy per particle

$$V_z \text{ in units of } V_{K0} = \sqrt{\frac{GM}{r_0}} = 94\left(\frac{M}{M_\Theta}\right)^{1/2}\left(\frac{r_0}{0.1AU}\right)^{-1/2} \text{km s}^{-1}$$

Zanni et al. (2007)

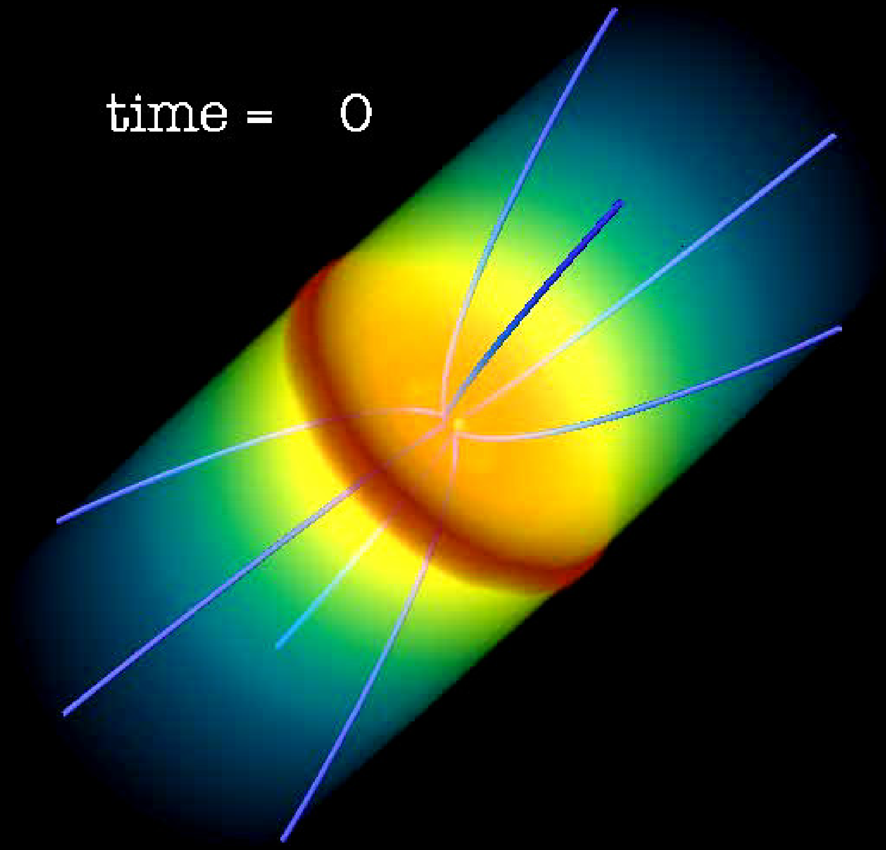

Density maps (logarithmic scale)   Unit time: $t0 = r_0/V_{K0} = 1.7\,\frac{(r_0/0.1AU)^{3/2}}{(M/M_\odot)^{1/2}}$ days

Size of the acceleration region

The acceleration region:

Size: 0.1- 1 AU ⟶ 0.7-7 mas

Problems to observations due to i) size and ii) extinction from disk matter

Contributions from VLTI observations to set constraints to *jet acceleration models*

Comparisons of models with observations

HH30 in the [SII] line

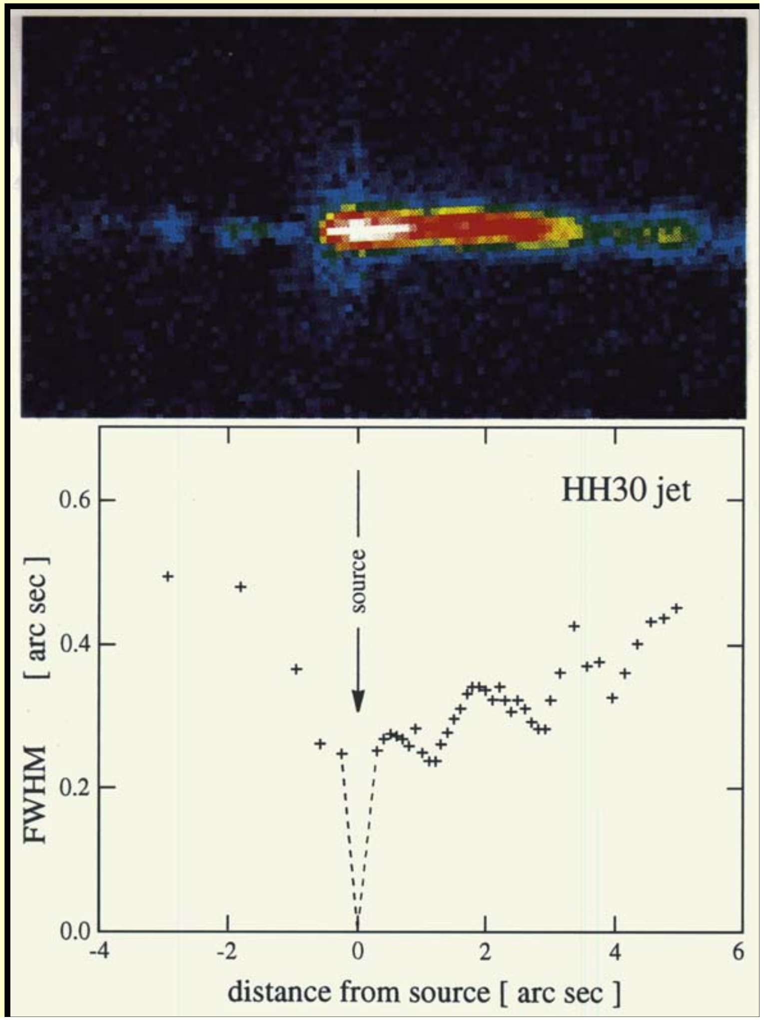

The present: comparisons with observations

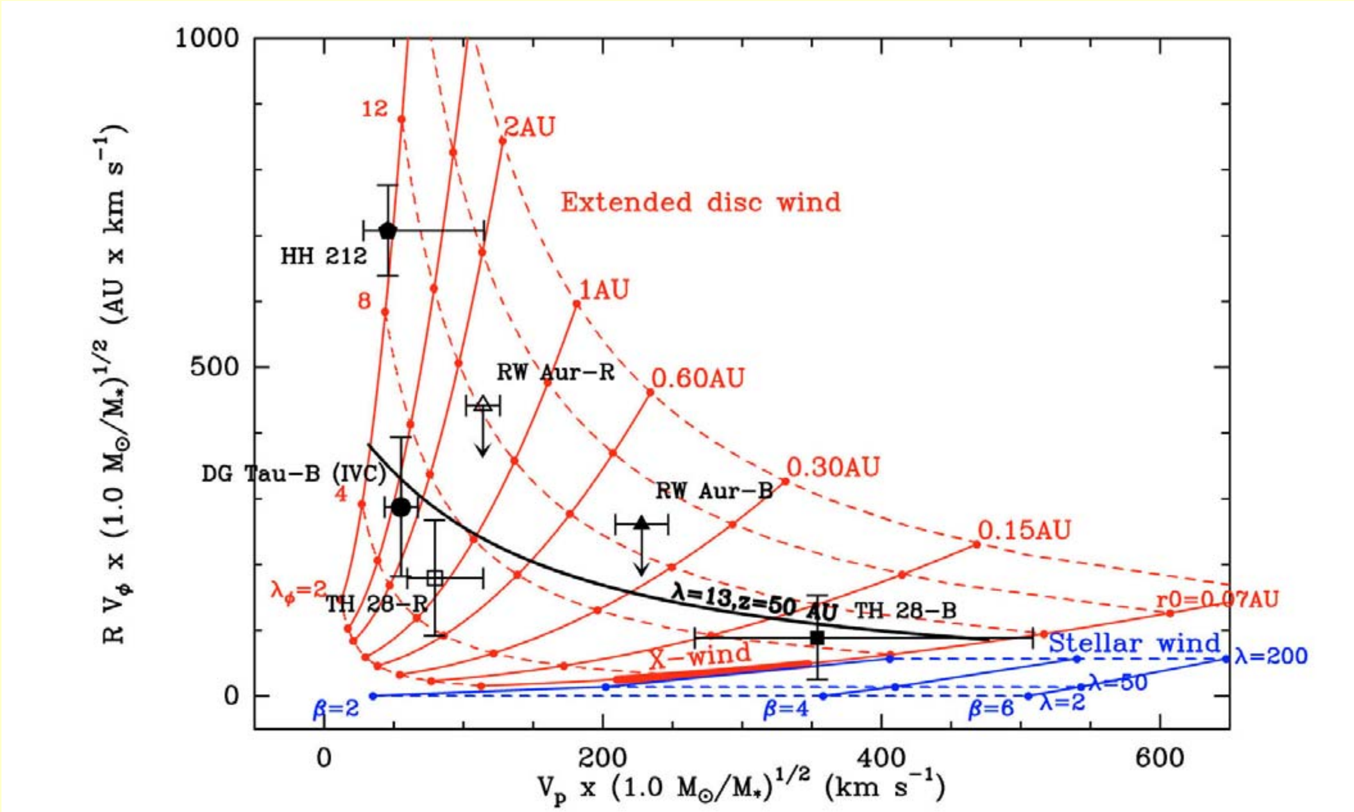

Magnetic lever arm: $\lambda = (r_A/r_0)^2$, r_A=Alfvènic radius, r_0=fiedline footpoint radius

Zanni et al. (2007): $\lambda \cong 9$

The present: comparisons with observations

Edwards et al. (2006) and Kwan et al. (2007):

observations of the line profiles of a sample of 39 CTTSs in the IR line HeI λ10830 and comparisons with the theoretical ones expected from stellar and disk wind models.

1) line profile characteristic of disk- winds in ~30% of the cases

2) characteristic of stellar winds in ~ 40% of the cases

The future: VLTI observations

Contributions from VLTI observations:

- **Set constraints to *jet acceleration models,* possibility of comparisons of models with observations by observing the circumstellar region where the jet acceleration takes place (with the near IR AMBER/VLTI instrument, Bacciotti et al. 2003, Thièbaut et al. 2003)**

- **Investigate possible connections between variations of the central star and formation of new knots in the jet**

- **Accurate measure of knots proper motions (up to 1 mas/day)**

Conclusions

- GMCs host young stars that emit jets;
- Jet emission spectra and observed morphologies can constrain the basic physical parameters;
- Jets are likely to be accelerated and collimated by MHD processes that take place about the accretion disk-central star region;
- Attempts to compare acceleration models with observations are under way;
- VLTI high resolution observation will better constrain and verify the acceleration mechanisms.